Acta Montanistica Slovaca
ISSN 1335-1788
actamont.tuke.sk

GIS-based assessment and mapping of groundwater source potential in selected aquifers of the Western Carpathians

Jozef MIŽÁK[1], Peter MALÍK[2], Marcela BINDZÁROVÁ GERGEĽOVÁ[3], Renáta PIJAKOVÁ[4] and Ivan KURIC[5]*

Authors' affiliations and addresses:
[1] State Geological Institute of Dionýz Štúr, Mlynská dolina 1, 817 04 Bratislava 11, Slovakia
e-mail: jozef.mizak@geology.sk

[2] State Geological Institute of Dionýz Štúr, Mlynská dolina 1, 817 04 Bratislava 11, Slovakia
e-mail: peter.malik@geology.sk

[3] Technical University of Košice, Faculty of Mining, Ecology, Process Control and Geotechnology, Institute of geodesy, cartography and geographical information systems, Park Komenského 19, 040 01 Košice
e-mail: marcela.bindzarova.gergelova@tuke.sk

[4] State Geological Institute of Dionýz Štúr, Mlynská dolina 1, 817 04 Bratislava 11, Slovakia
e-mail: renata.pijakova@geology.sk

[5] Faculty of Mechanical Engineering and Computer Science, University of Bielsko-Biala, ul. Willowa 2, 43-309 Bielsko-Biala, Poland
e-mail: kuric.ivan@gmail.com

***Correspondence:**
State Geological Institute of Dionýz Štúr, Department of Geofond, Mlynská dolina 1, 817 04 Bratislava 11, Slovakia
tel.: +421 2 593 75 325
e-mail: jozef.mizak@geology.sk

Funding information:
Funding Agency: KEGA
Grant Number: 055TUKE-4/2021

How to cite this article:
Mižák, J., Malík, P., Bindzárová Gergeľová, M., Pijaková, R. and Kuric, I. (2022). GIS-based assessment and mapping of groundwater source potential in selected aquifers of the Western Carpathians. *Acta Montanistica Slovaca*, Volume 27 (4), 1051-1077

DOI:
https://doi.org/10.46544/AMS.v27i4.18

Abstract
Using the frequency ratio (FR) statistical model can provide a simple geospatial assessment tool to calculate the probabilistic relationship between dependent and independent variables, including constructing multiple classification maps in a geographic information system (GIS) environment. A total of 10,465 springs were identified and mapped in the GIS environment during the research, including 5,302 in the Flysch Belt, 2,832 in the Crystalline complex, 351 in the Paleogene, and 1,980 in the Older Paleozoic. The effective factors - slope, aspect, plan curvature, elevation, topographic wetness index (TWI), stream power index (SPI), slope length (LS), lithology, distance to rivers, distance to ridge-lines, distance to faults, and distance to lithological borders - were derived from a spatial database. Using these effective factors, groundwater spring potential was calculated using a single model, and the results were plotted in ArcGIS. The final result indicated that the bivariate statistical index model (like FR) could be used as a simple tool in the assessment of groundwater spring potential.

Keywords
groundwater spring potential, geographic information systems, frequency ratio, logistics regression

Introduction

Groundwater is a strategic resource, and its importance will increase with climate change and gradual warming. We are already experiencing warm periods and declining groundwater levels. State Geological Institute of Dionýz Štúr (SGIDŠ) is an organization which provides geological research and exploration in the territory of the Slovak Republic. These activities' results were recorded and made available to the public through paper thematic maps and data. Generation of hydrogeological maps 1:50,000 was initially compiled in Slovakia by analogy with the previously used methodology of hydrogeological map compilation at the scale of 1:200,000 (Švasta, Malík, Mižák 2017). In 1991, a first draft methodology for compiling hydrogeological maps at a scale of 1:50 000 (Malík, Jetel, 1991; 1994) attempted to combine the strengths and eliminate the weaknesses of previous methodologies.

With computer technology and specialized software development, mapping has moved to an electronic environment. New methods of processing and evaluating data have thus emerged, as well as the possibility of modelling natural phenomena and looking for possible dependencies. With improvements in remote sensing (RS) and GIS technologies, these methods have become the standard procedure for mapping groundwater potential zones within each lithologic unit (Singh and Prakash, 2003). Many studies have been done on groundwater evaluation using GIS and RS (Ganapuram et al., 2009; Saha et al., 2010), potential groundwater mapping (Oh et al., 2011; Ozdemir, 2011b; Kaliraj et al., 2013; Pourtaghi, Pourghasemi, 2014; Naghibi, Dashtpagerdi, 2016; Ghimire, Chapagain, Shrestha, 2019; Nhu et al., 2020), evaluation of groundwater potential using probabilistic models Chenini et al., 2010; Chenini and Ben Mammou, 2010; Corsini et al., 2009; Gupta and Srivastava, 2010; Oh et al., 2011) or delineation of flood susceptibility zones (Vojtek, Vojteková, 2019, Blišťanová et al 2014, Kisss et al 2014).

The frequency ratio (FR) method is also applied to the problem of the susceptibility of the area to landslides and hazard mapping (Mohammady et al., 2012; Ozdemir and Altural, 2013; Regmi et al., 2013; Rasyid, A.R., Bhandary, N.P. & Yatabe, R., 2016; Nohani et al., 2019; Berhane et al., 2020; Gautam, Kubota, Sapkota, et al., 2021; Pham et al., 2021).

This report evaluates the mapping of groundwater source potential in selected areas of the Western Carpathians using the frequency ratio (FR) statistical model and GIS technique.

Study area and geological rock types

Crystalline

The crystalline area covers 3,312 km^2, which represents 6.75% of the total area of Slovakia (49,035 km^2). Lithology is formed by the rock types listed in Tab. 1, processed by GIS spatial analysis of the Digital Geological Map 1:50,000 (DGM) (Káčer et al.. 2005).

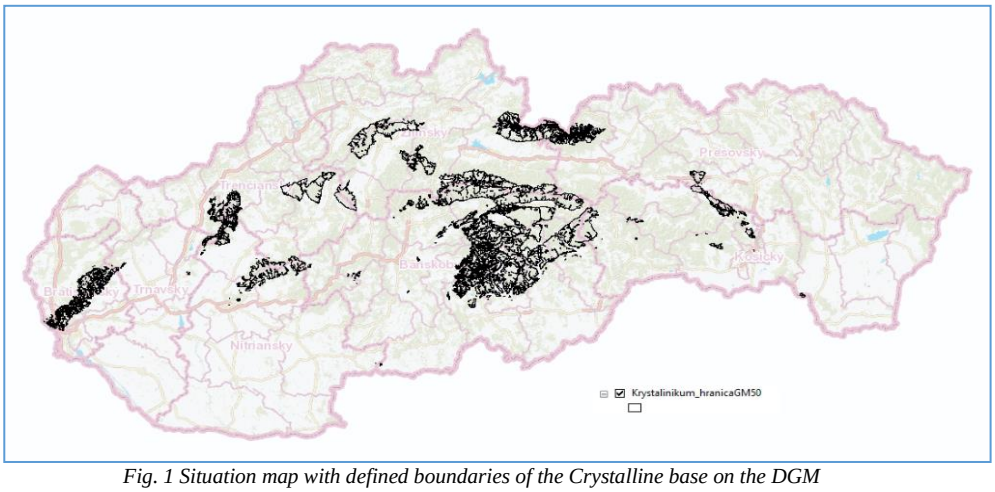

Fig. 1 Situation map with defined boundaries of the Crystalline base on the DGM

Tab. 1 Crystalline rock type based on the DGM

Code	Rock type	Code	Rock type
kr113	diaphthorised quartz-double-mica rubble	kr22	birefringent granites to granodiorites (Lipov type)
kr174	stromatitic-nebulitic and ophthalmitic migmatites	kr167	migmatitised orthorites, banded orthorites
kr5	light fine-grained aplitoid granites	kr115	diaphthoritised birefringent rules
kr2	aplitic granites	kr185	fine-grained biotitic rules and ophthalmitic migmatites with a substantial proportion of substrate

kr52	coarse-grained amphibolitic-biotitic and biotitic granodiorites	kr48	biotitic granodiorites
kr158	garnet-biotitic and garnet-sillimanitic rules, granulitic rules	kr74	hybrid granodiorites and tonalites
kr184	migmatites with relics of granulite facies metamorphites	kr134	muscovitic-chloritic svorites and svorite rulas
kr164	amphibolites	kr214	albitised chloritic (biotitic)-muscovitic alluvium ("albite rules")
kr112	diaphthorised feldspathic-quartz ores	kr166	pararules, quartzite ores to svorite ores with orthorhombic orthorhombic positions
kr110	diaphthorised fine-grained muscovite-quartz sills	kr127	chloritic-muscovitic welds
kr209	medium-grained, birefringent and muscovitic-tourmalinic granites	kr168	K-feldspar-plagioclase blastomylonitic orthorules (metagranitoids) meshed and banded
kr117	tectonic breccias	kr135	biotitic svoric rulas and pararuls
kr87	muscovitic-chloritic schists with metacarbonate and metabasic (Sinecky complex) positions	kr160	amphibolic rulas, amphibolites
kr50	biotitic granodiorites to tonalites (Modran type)	kr137	biotitic pararuls
kr97	phyllites, micaceous schists, metapelites of the biotite-granite zone	kr21	birefringent porphyritic granites (Zarya type)
kr147	biotitic pararulites with flake graphite	kr29	coarse-grained muscovitic-biotitic granites to granodiorites
kr94	graphitic-sericitic phyllites, graphitic metasediments	kr76	medium-grained biotitic granodiorites - hybrid tonalites with xenoliths of pararuls
kr162	fine- to medium-grained amphibolites (Pesina succession)	kr151	granitic-biotitic pararuls
kr26	medium-grained leucocratic muscovitic and birefringent granites, granodiorites (Bratislava type)	kr45	porphyritic granodiorites mainly with white K-feldspar outgrowths (Vepor type)
kr35	coarse-grained muscovitic, muscovitic-biotitic granites, granodiorites rich in pegmatites (Bratislava type)	kr199	bright feldspathic orthorules with muscovite-chlorite-granatite svorites and amphibolites (Murano granorules)
kr17	leucocratic fine-grained biotitic and birefringent granites to granodiorites	kr181	migmatites, orthorules, strongly oriented hybrid granitoids and positions of pararules (hybrid complex)
kr66	birefringent granitoids (Modran type)	kr78	biotitic granodiorites to tonalites (hybrid type): oriented or omnidirectional, locally porphyritic
kr91	actinolitic schists	kr116	diaphthorites and tectonites mostly svoric, often with garnet
kr176	oriented granitoids (biotitic-muscovitic orthorites)	kr55	biotitic granodiorites to tonalites with transitions to muscovitic-biotitic granodiorites (High Tatra type)
kr145	biotitic and muscovitic-biotitic pararuls weakly migmatitised	kr9	leucocratic granites
kr63	biotitic tonalites to granodiorites (Spruce type)	kr43	biotitic and birefringent granodiorites with pink K-feldspars (Powderian type)
kr31	biotitic granodiorites to muscovitic-biotitic monzogranites with pink K-feldspars (Korniet type)	kr178a	orthorules and migmatized orthorules with banded or banded texture, predominantly mylonitized
kr15	leucocratic, muscovitic, ± biotitic-muscovitic granites to granodiorites (Lubochnian type)	kr57	tonalites (rarely biotitic granodiorites)
kr1	pegmatites and aplites	kr136	fine-grained biotitic pararules

Paleozoic

The Older Palaeozoic covers 1,005 km^2, which represents 2.05% of the total area of Slovakia. Lithological types are listed in Tab. 2.

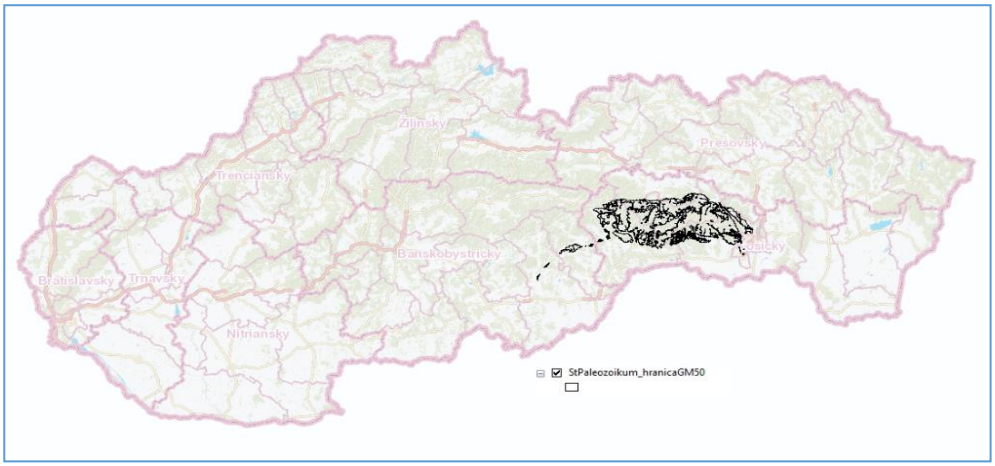

Fig. 2 Situation map with defined boundaries of the Paleozoic base on the DGM

Tab. 2 Paleozoic rock type based on the DGM

Code	Rock type	Code	Rock type
ps18	metabasalt tuffs and tuffites	ps57	predominantly coarse-grained metaryolite tuffs
ps19	phyllites with interbedded metabasalt tuffs and tuffs	ps60	metamorphosed quartz clasts predominantly over quartz phyllites
ps74	coarse-grained metaryolite tuffs	ps53	finely laminated quartz-sericitic and graphitic-sericitic phyllites
ps75	metaryolites and metaceratophyres	ps56	medium-grained metaryolite tuffites
ps65	hidden-layered sericitic-graphitic phyllites	ps61	coarse-grained and rhythmically laminated metamorphosed quartz clasts
ps29	quartz phyllites with metamorphosed sandstones	ps59	quartz phyllites overlying metamorphosed quartz clasts
ps30	metamorphosed sandstones	ps50	metalloidites
ps27	metabasalt tuffs and tuffs	ps51	covertly bedded sericitic-graphitic phyllites, locally with impregnations of pyrite
ps8	gabrodiorites	ps70	metabasalt tuffs and tuffs
ps23	metabasalts, spilites and green shales	ps44	metaryolites and metaceratophyres
ps9	amphibolites and rules	ps48	microconglomerates
ps24	actinolitic schists with interbedded dark phyllites	ps37	greenish quartz phyllites
ps76	laminated quartz phyllites in equilibrium with or overlying metamorphosed quartz clasts	ps62	microconglomerates
ps77	rhythmically foliated metamorphosed quartz clasts	ps54	actinolitic schists
ps64	metalloidites	ps45	quartz phyllites overlying metamorphosed quartz clasts
ps67	finely laminated quartz-sericitic and chloritic-sericitic phyllites	ps17	sericitic-chloritic phyllites
ps83	products of bimodal volcanism	ps16	quartz-sericitic phyllites
ps82	flysch sandstones	ps34	hidden-layered graphitic and sericitic-graphitic phyllites
ps66	unlaminated, sporadically laminated greenish quartz phyllites and sericitic-chloritic phyllites	ps13	laminated sericitic-chloritic phyllites
ps72	metaryolite tuffs with elevated chlorite content	ps12	grey sericitic phyllites
ps73	fine-grained metaryolite tuffites	ps33	metalydites
ps68	metamorphosed quartz clasts overlying quartz phyllites	ps52	unlaminated, sporadically laminated sericitic-chloritic phyllites
ps43	coarse-grained metaryolite tuffs	ps40	metabasalts
ps36	laminated chloritic-sericitic and graphitic-sericitic phyllites	ps85	olive green phyllites
ps47	metamorphosed quartz clasts	ps25	metaryolites
ps46	metamorphosed quartz clasts overlying quartz phyllites	ps28	quartz-sericitic phyllites
ps41	metaryolite tuffs with elevated chlorite content	ps2	metabasaltic tuffs and tuffites
ps39	metabasaltic tuffs and tuffs	ps6	sericitic, sericitic-chloritic and graphitic phyllites
ps42	fine-medium-grained metaryolite tuffites	ps3	metabasalts, doleritic metabasalts, green shales, local epidote amphibolites
ps35	predominantly unlaminated, rarely laminated sericitic-chloritic phyllites	ps14	metamorphosed sandstones with quartz phyllites

Paleogene

The area of interest of the Inner Carpathian Paleogene covers 2,899 km^2, which represents 5.91% of the total area of Slovakia. Lithological types are listed in Tab. 3.

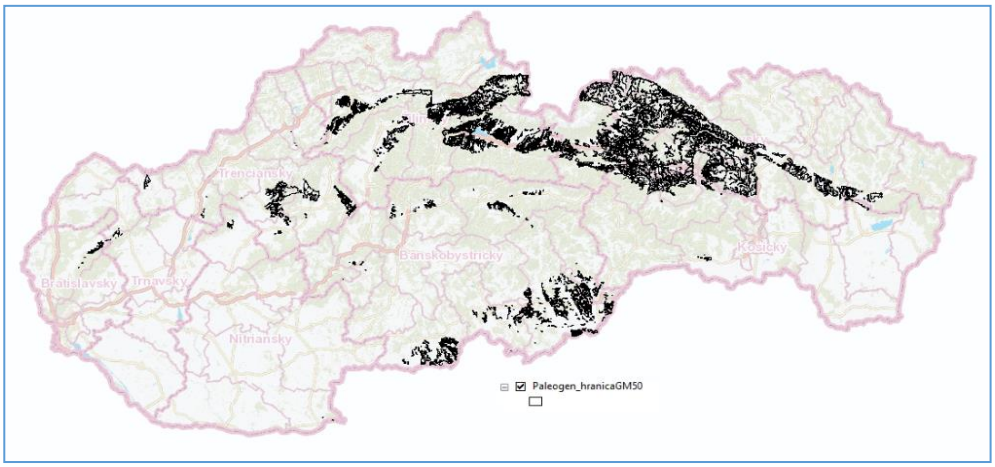

Fig. 3 Situation map with defined boundaries of the Paleogene base on the DGM

Tab. 3 Paleogene rock type based on the DGM

Code	Rock type	Code	Rock type
pg7	Tomáš beds: fine-grained sandstones and silts	pg25	conglomeratic flysch: thick benches of polymictic conglomerates, thin beds of sills to claystones
pg4c	polymictic conglomerates	pg13a	fine-rhythmic flysch or claystones
pg5	Hornád beds: polymictic conglomerates, coarse-grained sandstones	pg10	Tertiary (marginal) strata: breccias, conglomerates, sandstones
pg6	Chrastian beds: obliquely bedded sandstones, lenses of conglomerates	pg4a	Pine Formation - lower part not dissected: breccias, conglomerates, sandstones, siltstones, limestones
pg19	Kezmare beds: coarse benches sandstones, thin beds of claystones	pg17	Hutian - Zuberecan stratum, unarticulated
pg23	medium- and coarse-grained sandstones in absolute predominance over claystones	pg17a	positions of flysch character
pg18	normal flysch: claystones, silts and sandstones	pg41a	Abbot beds: calcareous siltstones to clays with thin coal seams
pg4b	carbonate breccias, conglomerates and sandstones	pg37	Szeczen shale: calcareous silts - silts, with occasional sand and clay beds
pg2a	carbonate breccias and conglomerates	pg8	organogenic and organodetrital limestones and sandy limestones
pg3	bauxites	pg40	Breccia beds: detrital and organodetrital limestones, conglomerates and breccias
pg2b	polymictic conglomerates	pg20b	flysch dominated by sandstones
pg12	claystones in absolute predominance over sandstones and conglomerates		

Flysch zone

The area of interest of the flysch zone covers 5,829 km^2, which represents 11.89 % of the total area of Slovakia. However, only the eastern part was used for the purposes of the dissertation, as the input data was only from this part. The eastern part represents an area of 3,575 km^2, i.e. 7.29 %. Lithological types are listed in Tab. 4.

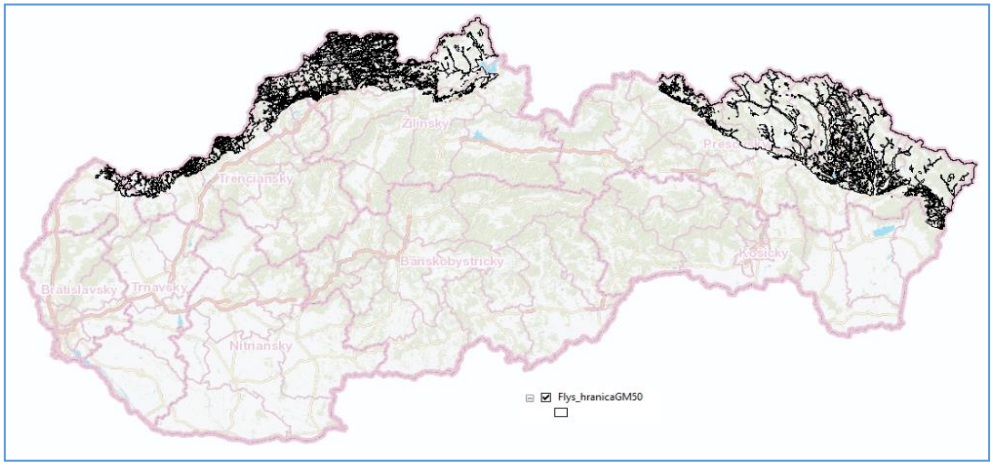

Fig. 4 Situation map with defined boundaries of the Flysch zone base on the DGM

Tab. 4 Flysch zone rock type based on the DGM

Code	Rock type	Code	Rock type
f84	carbonate sandstones, conglomerates, claystones, siltstones (carbonate flysch)	f116	Cisnian beds: medium- and coarse-grained fine sandstones, fine-grained conglomerates, grey sandy claystones (sandy flysch)
f56	'Older Maltsovian Formation': sandstones with claystones, fine-grained conglomerates (coarse-sammonitic flysch)	f9	Lupka Formation: dark claystones, calcareous claystones, silts and fine-grained sandstones
f43	calcareous claystones, sandstones (flysch)	f17	green, grey and brown calcareous claystones, fine- to medium-grained fine sandstones (thin-bedded flysch)
f5	conglomerates with 'exotic material'	f12	predominantly red and green claystones, fine-grained fine sandstones
f85	red and grey-green sandy clays, Mn concretions, thin-bedded sandstones	f49	black and brown claystones, sandy claystones, fine sandstones, slip bodies, occasional pelocarbonates
f53	grey calcareous claystones and sandstones with inclusions of menilite-type claystones	f118	Cergow flysch beds: calcareous grey, ochre and brown claystones, calcareous fine-grained sandstones
f34	'variegated beds' and globigerine sills: variegated claystones, Mn concretions, sandstone interbeds	f46	hornfels and weathered claystones
f69	Passier Sandstones: green and white quartz and arkosic sandstones with glauconite, rarely bustritic claystones	f117	cergow sandstone beds: calcareous coarse-grained sandstones, grey and ochre claystones
f86	polymictic conglomerates, microconglomerates ('Prochian conglomerates')	f10	Papinean beds: grey and ochre calcareous claystones and fine-grained sandstones with interbeds of menilitic claystones and organodetrital sandstones
f31	variegated claystones with benches of calcareous sandstones	f116	Cisnian beds: medium- and coarse-grained fine sandstones, fine-grained conglomerates, grey sandy claystones (sandy flysch)
f84	carbonate sandstones, conglomerates, claystones, siltstones (carbonate flysch)	f9	Lupka Formation: dark claystones, calcareous claystones, silts and fine-grained sandstones
f56	'Older Maltsovian Formation': sandstones with claystones, fine-grained conglomerates (coarse-sammonitic flysch)		

Methodology

Data

In the first step, it was necessary to select sources located in the areas of interest from the database of primary data. The database of primary source data contains 34,366 records from all over Slovakia. The following data were recorded during the documentation of springs, like spring number on the docking point map, name of the locality in which the spring is located, lithological and stratigraphic index of the rock environment drained by the spring, elevation of the spring, spring discharge (single measurement), spring water temperature (single measurement), date of measurement of discharge and water temperature, date of any sampling, specific electrical conductivity, and a note on the eventual capture or use of the spring. Each record contains 39 attributes.

As the first step, using extensive field surveys, 10,465 springs were detected in the study areas and were mapped (Fig. 5). For Flysch zone 5,302, for Crystalline 2,832, Paleogene 351 and for Paleozoic 1,980 springs were detected (Tab. 5).

Tab. 5 Springs data in study areas

	Flysch	Crystalline	Paleogene	Paleozoic
Springs	5,302	2,832	351	1,980
Area km^2	5,829.33*	3,312.29	2,899.44	1,004.70
Number on km^2	1.48*	0.85	0.12	1.97

**The area has been adjusted to 3,575 km^2 as the input data was only from the eastern part*

Effective factors

Different authors use different effective factors in their works. Pourthagi and Pourghasemi (2014) have used in their work slope angle, slope aspect, elevation, topographic wetness index (TWI), stream power index (SPI), slope length (LS), plan curvature, lithology, land use, and distance to river, road, fault. Naghibi and Dashtpagerdi (2016) used elevation, slope angle, plan curvature, profile curvature, slope length, TWI, SPI, distance from the river, rivers density, distance from faults, faults density, land use and lithology or Ghamire, Chapagain and Shrestha (2019) used eleven effective factors like elevation, slope gradient, slope shape, relative relief, flow accumulation, runoff density, geology, line density, land use and vegetation density.

In this study were used 12 effective factors to create a spring potential map (SPM) like slope, aspect, plan curvature, elevation, topographic wetness index (TWI), stream power index (SPI), slope length (LS), lithology, distance to rivers, distance to ridge-lines, distance to faults, and distance to lithological borders. Slope, aspect, plan curvature and elevation were derived using a Digital Elevation Model (DEM) of the area in GIS.

Slope

Minár and Machová (2010) define the slope of the georelief in the bedding direction as a key morphometric parameter determining the instantaneous intensity of gravity-driven geomorphological processes. Its value depends on the normal force, attracting a massive particle (boulder, snow, etc.) to the slope surface and thus increasing the frictional force of its movement along the slope (it decreases with increasing slope gradient), as well as the force acting in the direction of slope gradient against the stability of the particle and inducing its downward movement (it increases with increasing slope gradient). The slope of a georelief in a topographic map is expressed by the distance of adjacent contours. In areas of constant elevation (without contours) and at all singular points, the slope of the georelief is zero. A simple qualitative estimate of the slope of the area can be made by looking at a topographic map - in the areas with the densest contours; the slopes are maximal. In the minimally sloping areas, the contours are further apart. Table 6 shows the derived slope values for each aquifer in degrees.

Tab. 6 Slope based on DEM

	Slope (gradient)			
	Flysch	Crystalline	Paleogene	Paleozoic
Min	0.00	0.00	0.00	0.00
Max	66.23	83.75	60.35	56.91
Avg	33.115	41.875	30.175	28.455

Aspect

The aspect identifies the downslope direction of the maximum rate of change in value from each cell to its neighbours. It can be thought of as the slope direction. The values of each cell in the output raster indicate the compass direction that the surface faces at that location. It is measured clockwise in degrees from 0 (due north) to 360 (again due north), coming full circle. Flat areas having no downslope direction are given a value of -1. Table 7 shows the aspect of springs based on DEM in study areas.

Tab. 7 Aspect

	Slope (gradient)			
	Flysch	Crystalline	Paleogene	Paleozoic
Flat	0	0	0	0
North	384	338	49	276
North-east	578	399	42	276
East	728	353	43	301
Southeast	630	309	35	293
South	765	337	50	187
South-west	986	358	45	158
West	686	325	48	188
North-west	545	413	39	301

Plan curvature

The Planform curvature (commonly called plan curvature) is perpendicular to the direction of the maximum slope. Planform curvature relates to the convergence and divergence of flow across a surface.

Elevation

The elevations of the study areas are shown in Tab. 8 and Tab. 9. Based on the data analysis, errors were found in the measured data, and hence a correction was made based on the DEM. Table 10 shows the differences in elevation between the measured and DEM-derived elevations.

Tab. 8 Spring elevation from the database - Min – minimum, Max – maximum, Avg – average, Med – median

	Elevation [meters above sea level]			
	Flysch	Crystalline	Paleogene	Paleozoic
Min	265.00	155.00	164.00	57.00
Max	1,120.00	2,160.00	1,018.00	1,665.00
Avg	650.91	738.06	497.85	755.16
Median	638.00	675.00	495.00	760.00

Tab. 9 Elevation DEM 3.5

	Elevation [meters above sea level]			
	Flysch	Flysch zone	Flysch zone	Flysch zone
Min	259.42	155.46	168.14	357.83
Max	1,135.45	2,221.50	1,011.88	1,218.18
Avg	651.84	741.60	501.08	756.93
Median	640.55	678.51	494.51	760.54

Tab. 10 Differences in values between measured altitudes and DEM 3.5

	Elevation [meters above sea level]			
	Flysch	Flysch zone	Flysch zone	Flysch zone
Min	-5.58	0.46	4.14	300.83
Max	15.45	61.50	-6.12	-446.82
Avg	0.93	3.55	3.23	1.77
Median	2.55	3.51	-0.49	0.54

Analysis of the elevation data revealed an error that occurred during data collection. Therefore, in further analyses, the data from DEM will be used.

Topographic wetness index (TWI)

The topographic wetness index (TWI), also known as the composite topographic index (CTI), is a steady-state moisture index. It is commonly used to quantify the topographic control of hydrologic processes. TWI was developed by Beven and Kirkby (1979) as part of a runoff model. It is defined as:

$$TWI = ln\frac{a}{tan\, b} \qquad (1)$$

where a is the rising area (m^2) and b is the slope of the area in radians.

Stream power index (SPI)

The Stream Power Index (SPI) can be used to describe the potential erosion of a stream at a given point on a topographic surface. As the watershed area and slope gradient increase, the amount of water contributed by the slope area and the velocity of water flow increases, thereby increasing the Stream Power Index and the risk of erosion. De Rosa, Fredduzzi, and Cencetti (2019) defined the calculation as follows:

$$\Omega = \rho * g * Q * S \tag{2}$$

where

Ω - flow power per unit flow length (W/m),
ρ - density,
g - gravitational acceleration,
$\rho * g$ - specific gravity of the fluid (kg/m^3),
Q - fluid flow rate (m^3/s) and
S - slope of the section under consideration (m/m).

Slope length (LS)

Hickey (2000) describes the calculation of slope length as part of the calculation of the universal soil loss equation. This is a combination of the flow direction (flow direction) and the slope gradient. Moore and Burch (1986) calculated as:

$$LS = \left(\frac{B_S}{22.13}\right)^{0.6} \left(\frac{\sin \alpha}{0.0896}\right)^{1.3} \tag{3}$$

Fig. 5 shows the maps produced by the GIS tools based on the DEM for the flysch zone. The same methodology was used to create maps for the Crystalline, Paleogene, and Paleozoic regions and combine them to create maps of the spatial relationships between effective factors and spring locations using the FR model based on GIS. Detailed data are shown in Tab. 9 to Tab. 13.

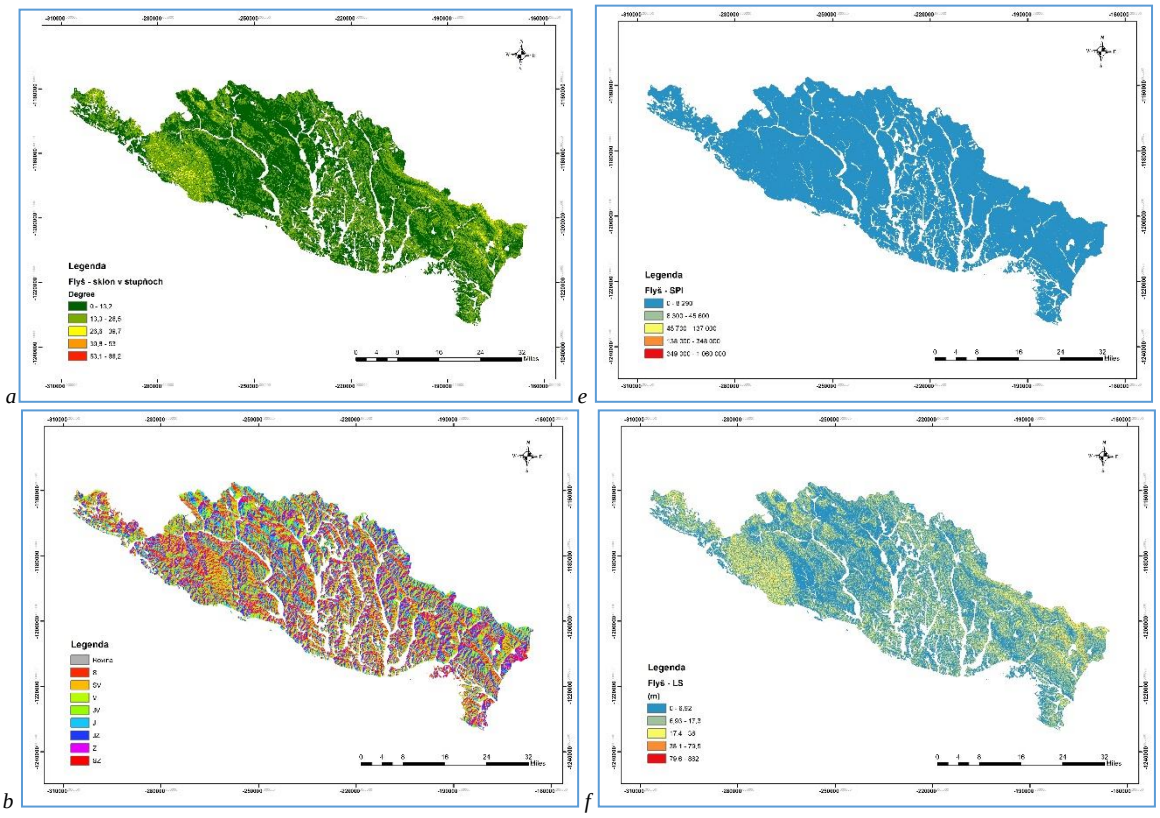

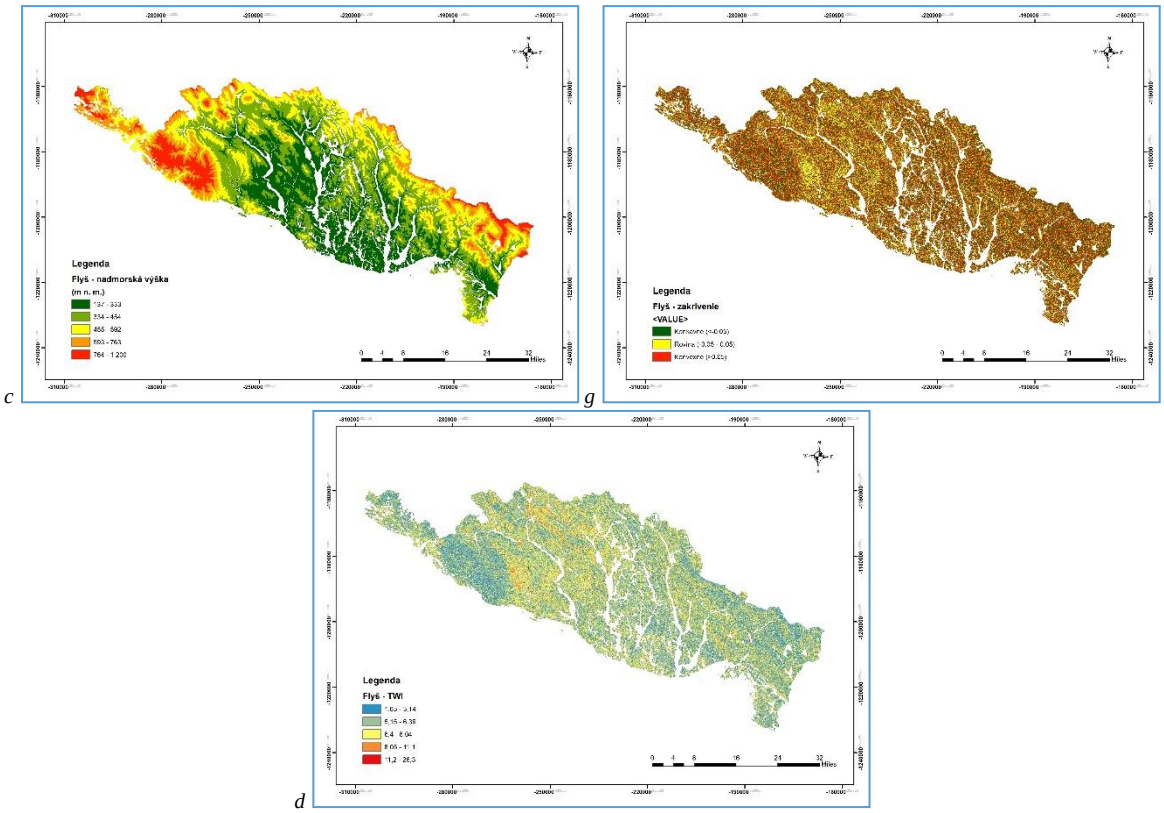

Fig. 5 Effective parameters maps of Flysch zone: a – slope (degree), b - aspect, c - elevation (meters above sea level), d - TWI, e - SPI, f - LS, g – plan curvature

Distance

Distance analyses were created in the ArcGIS environment based on using Euclidean distance. Maps of distance to faults (Fig. 6a) and lithology interfaces (Fig. 6b) were created based on data from the DGM. Maps of distances to river and ridge-lines (Figs. 6c, 6d) were created from the DEM.

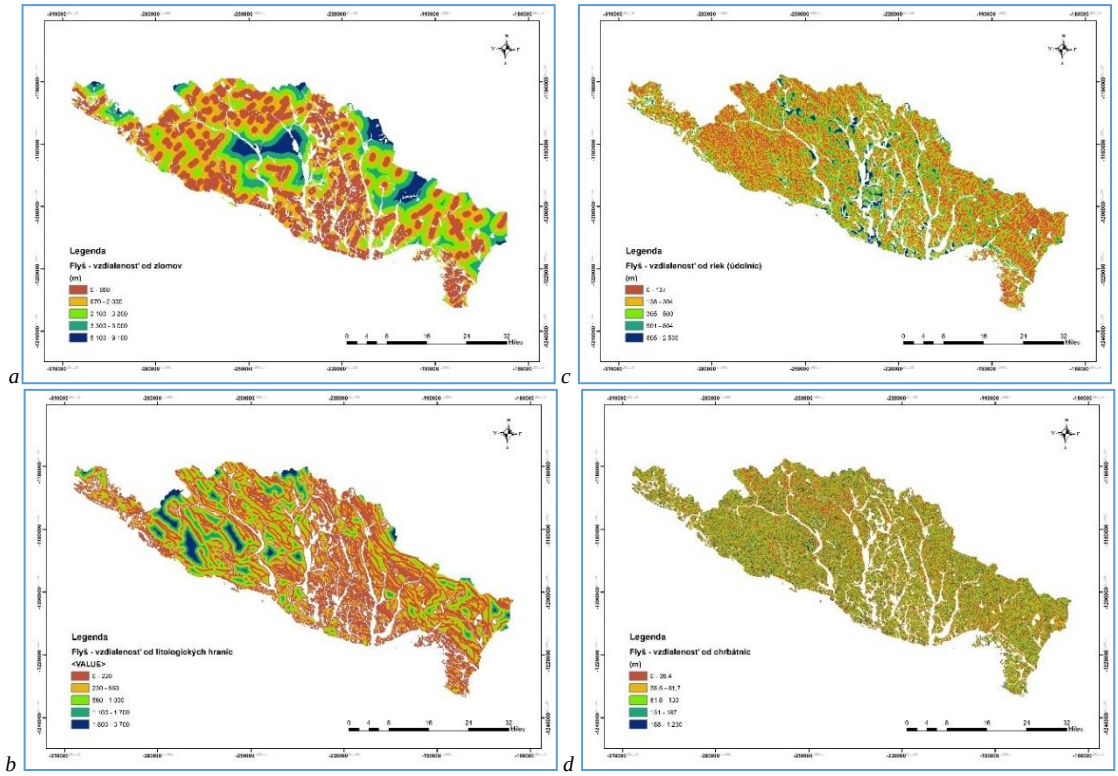

Fig. 6 Distance to: a - faults (buffer), b – litological borders (buffer), c - rivers (buffer), d – ridge-lines (buffer)

Frequency ratio, Relative frequency, Prediction Rate and Susceptibility Index

The frequency ratio (FR) method is one of the most commonly used probabilistic models in susceptibility studies due to its simplicity (Wu et al., 2016; Kayastha, 2015; Regmi et al., 2013; Choi et al., 2012; Yilmaz, 2009; Lee and Sambath, 2006). FR is defined as the ratio of the area where the phenomenon under study occurred to the total area under study and is also the ratio of the probabilities of occurrence of a phenomenon and its non-occurrence for a given attribute (Bonham-Carter, 1994; Lee and Sambath, 2006; Pradhan and Lee, 2010). It is based on the observed relationship between the spatial distribution and causal factors of phenomena and can be expressed mathematically as:

$$FR = \frac{N_{pix}(LX_i) \Big/ \sum_{i=1}^{m} N_{pix}(LX_i)}{N_{pix}(X_j) \Big/ \sum_{j=1}^{n} N_{pix}(X_j)} \quad (4)$$

where

FR is the frequency ratio of class *i* parameter *j*. $N_{pix}(LX_i)$ is the number of pixels with the phenomenon under study within class *i* and the variable parameter *X*. $N_{pix}(X_j)$ is the number of pixels within the variable parameter X_j, *m* is the number of classes in the variable parameter X_i and *n* is the number of parameters in the study region (Regmi et al., 2013).

Based on a range of probability values [0,1], the *FR* values are normalized as Relative Frequency (*RF*), expressed as:

$$RF = \frac{FR_{ij}}{\sum_{i=1}^{m} FR_{ij}} \quad (5)$$

After normalization, the *RF* frequency still has a disadvantage - all conditioning factors are considered equally severe. In order to resolve this disadvantage and account for the interrelationships between the independent variables, a prediction rate (*PR*) function is used, expressed as:

$$PR = \frac{(RF_{max} - RF_{min})}{(RF_{max} - RF_{min})_{min}} \quad (6)$$

The susceptibility index (*SI*) expresses the sum of the product of the prediction function of each factor of each class:

$$SI = \sum (PR * RF) \quad (7)$$

A susceptibility map for the phenomenon under study was created based on the SI values. The *SI* value is used as an individual weight for all parameters.

Based on the *FR* values, the relative frequency (*RF*) can be calculated, followed by the prediction function (*PR*) and finally, the susceptibility index - the ratio values obtained using the *FR* were assigned as class weights (Tab. 12) to each factor map to create topic-weighted factor maps, which were overlaid and numerically summed using a raster calculator to create the susceptibility index map (Fig. 10).

The susceptibility indices of the area were classified into 5 susceptibility classes, namely 1) very low; 2) low; 3) medium; 4) high; 5) very high.

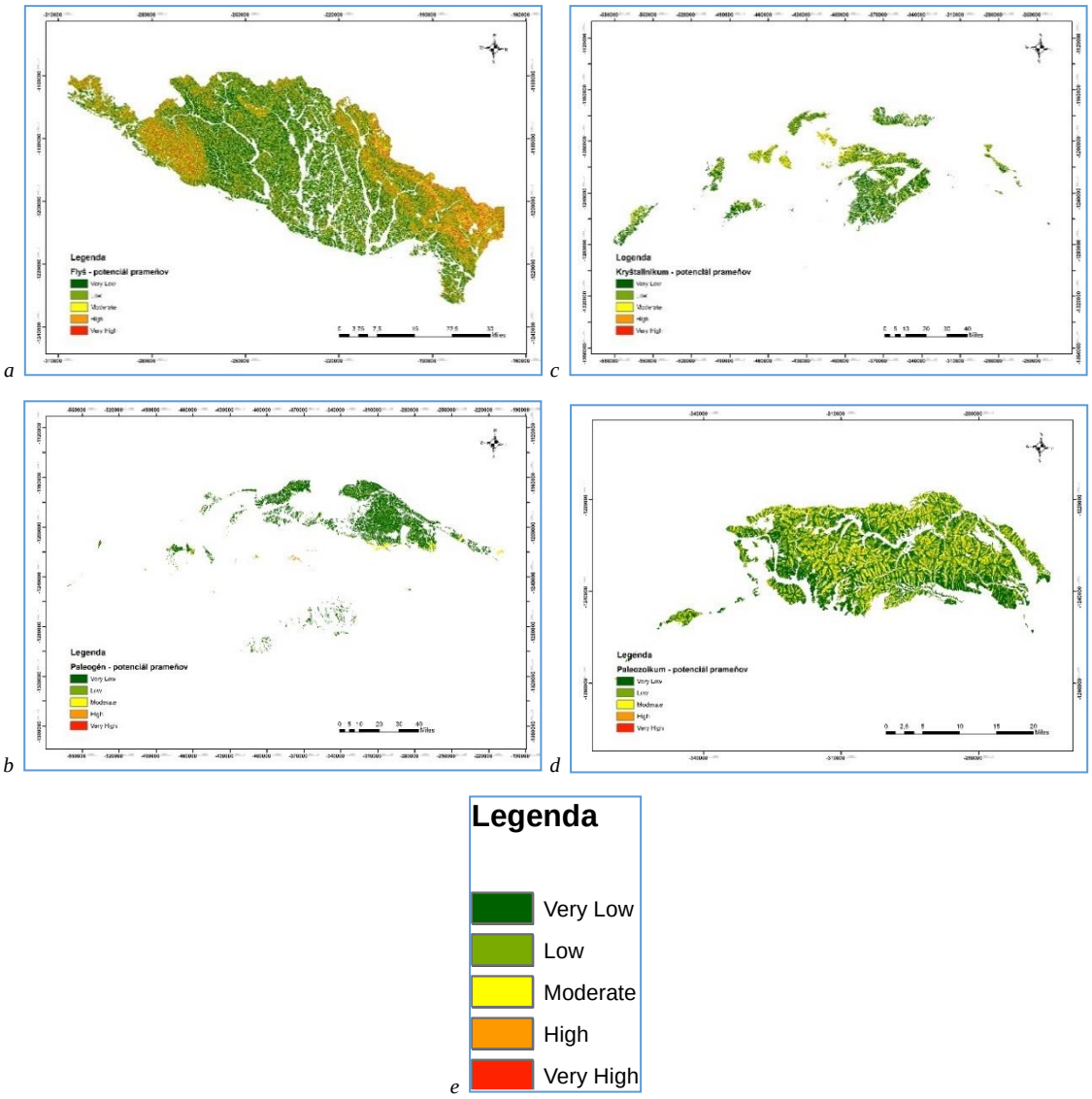

Fig. 10 Prediction map GIS-based groundwater potential mapping in a - Flysch zone, b - Palaeogene, c - Crystalline, d - Palaeozoic, e - 5 Susceptibility classes

If the susceptibility index is converted to an area representation, then we get the values shown in Table 11.

Tab. 11 Area expression of the susceptibility index

SI	Area [km^2]			
	Paleozoic	Paleogene	Crystalline	Flysch
1 – Very Low	565.79	1,231.45	1,644.12	1,270.81
2 – Low	217.34	799.78	722.55	921.36
3 – Moderate	182.17	685.20	734.67	654.75
4 – High	26.32	94.38	110.72	478.60
5 – Very High	4.40	11.28	51.32	213.08
6 – No Data	8.99	76.90	48.62	36.40

Tab. 12 Weighting of the susceptibility index

Class	Flysch	Crystalline	Paleozoic	Paleogene
Slope (degree)	10.88	1.73	1.00	2.93
Aspect	1.00	1.00	1.01	1.00
Plan curvature	15.11	10.01	5.18	9.45
Elevation	7.93	3.42	1.33	4.57
Distance to Fault	4.39	4.33	3.09	4.22
Distance to Lithological borders	3.44	5.15	1.49	6.62
Distance to river	10.89	8.57	5.06	3.13

Distance to ridge-lines	8.86	3.92	1.53	10.19
TWI	4.51	3.28	8.57	6.57
SPI	13.41	9.19	4.70	11.56
LS	11.97	2.99	1.66	3.43
Geological type	11.69	5.67	1.27	8.45

As shown in Tab. 12 and Charts (1-4), for both the Flysch zone and the Crystalline zone, the highest weight was calculated for the plan curvature data. For the Paleozoic, it was the TWI, and for the Paleogene, it was the SPI.

Conversely, the lowest values were calculated for aspect (Flysch, Crystalline, Paleogene). For the Paleozoic, the slope was calculated to be the lowest factor, but only just ahead of the aspect.

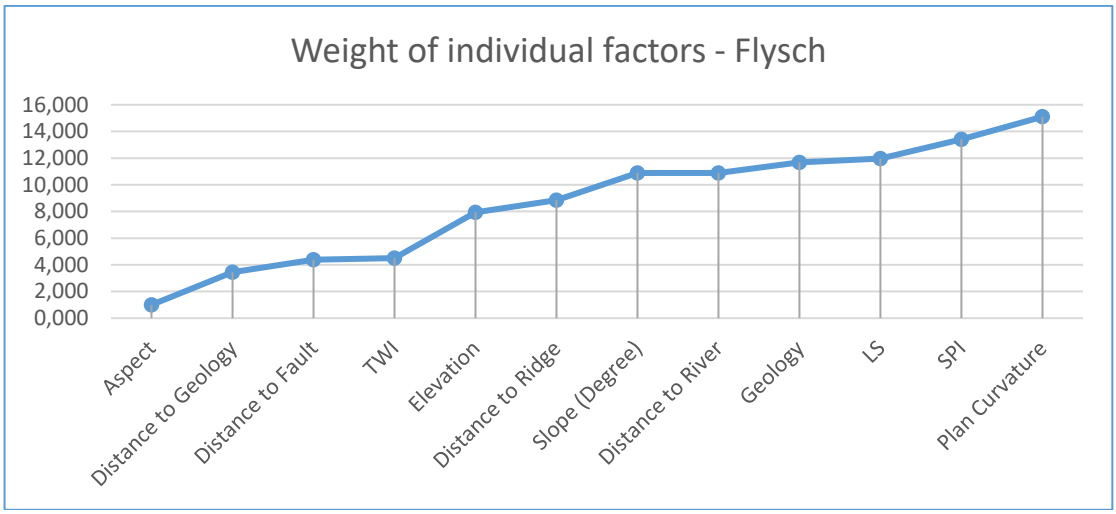

Chart 1 Weighting of individual factors – Flysch

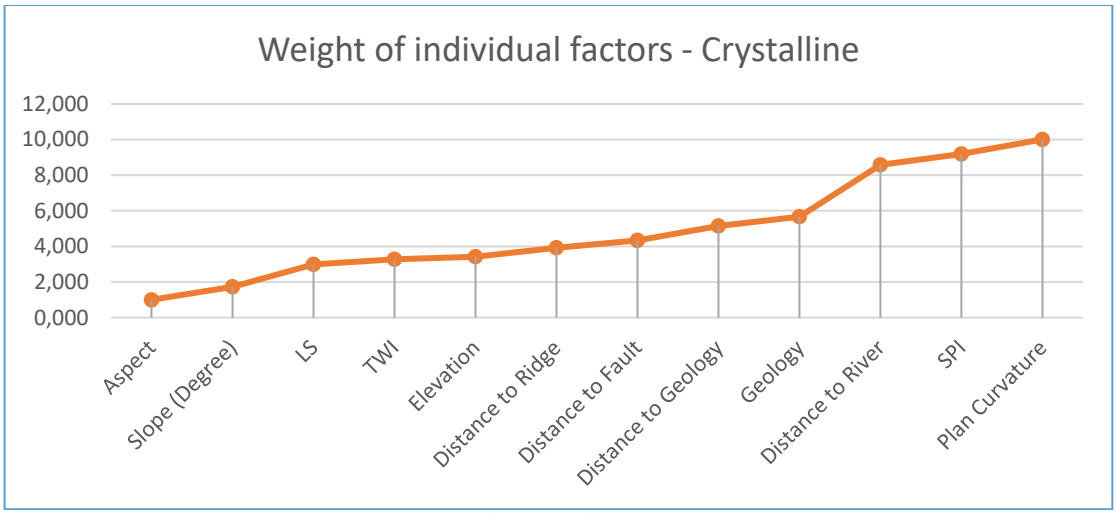

Chart 2 Weighting of individual factors - Crystalline

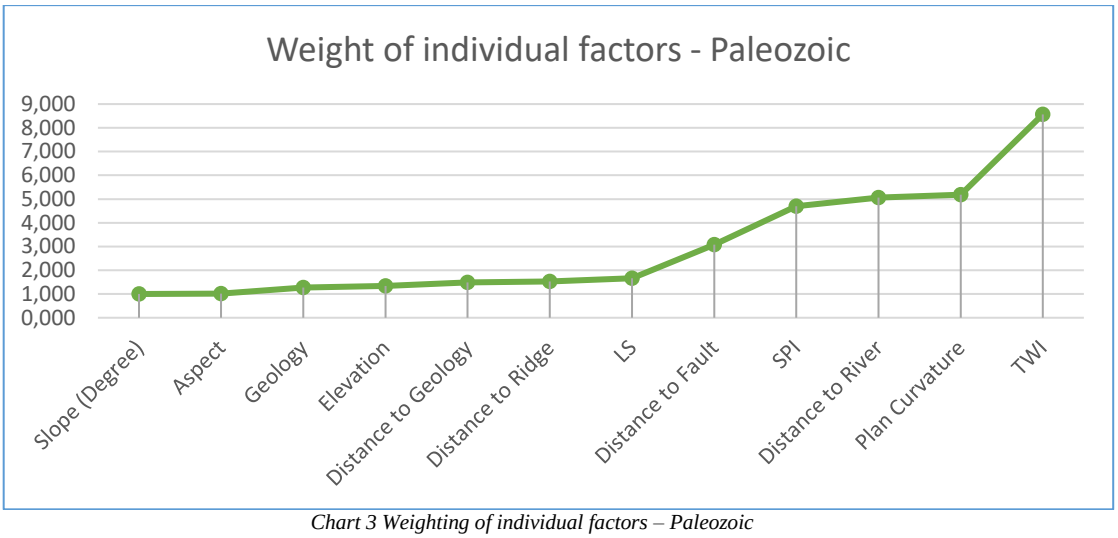

Chart 3 Weighting of individual factors – Paleozoic

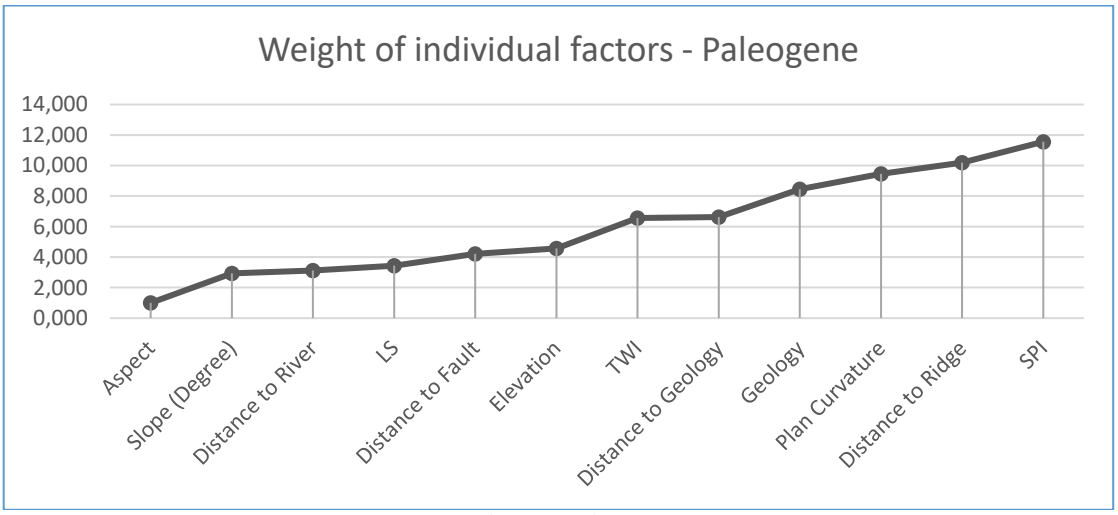

Chart 4 Weighting of individual factors - Paleogene

Results

Frequency ratio

The spatial relationship between each effective factor and spring location using the FR model is presented in Tab. 14 – 17 for each location. The ratio of the area where springs occurred to the total area was calculated. There is a high correlation if the FR value is larger than 1 and a lower correlation if the FR value is less than 1 (Pourthagi, Pourghasemi 2014).

Flysch zone

Analysis of the FR result shows that the ratio is <1 for a slope of <15° and > 45°, indicating a low probability of spring occurrence within this slope range. The ratio is >1 for slopes more than 15° to 45°, which indicates a high probability of spring occurrence. Springs are most abundant on the southeast (112.5-157.5°) and north-west facing (292.5-337.5°), considering the relationship between spring occurrence and aspect. In the case of plan curvature, the results showed that the concave shape yielded the highest FR value 1.97, and convex shapes had the lowest value (0.52). In the study area, where topographic elevation is between 920 m and 1 200 m, the FR is high (values of 4.21). Results based on distance analyses showed that FR >1 for 2,100 – 2,700 m (distance to fault), 1,500 – 1,800 m (distance to lithology borders), 1 m (distance to the river) and 506 – 1,230 m from distance to ridge-lines. In the case of lithology, group 6 yields an FR value of 3.18. Thus, it has the highest probability of spring occurrence. Detailed results are in Tab. 14.

Crystalline

Analysis of the FR result shows that the ratio is <1 for a slope more than >33.9°, indicating a low probability of spring occurrence within this slope range. The ratio is >1 for slopes more than 0° to 33.8°, which indicates a

high probability of spring occurrence. The highest value was calculated for slope class 9.21-14.8° (1.36). Springs are most abundant in the north-west (292.5-337.5°), considering the relationship between spring occurrence and aspect. In the case of plan curvature, the results showed that the concave shape yielded the highest FR value 3.41, and convex shapes, the lowest value (0.47). In the study area, where topographic elevation is between 459 m and 656 m, the FR is high (values of 1.56). Results based on distance analyses showed that FR >1 for <925 m (distance to fault); 1,400 – 2,310 m (distance to lithology borders); <183 m (distance to the river), and 763 – 1,550 m from distance to ridge-lines. In the case of lithology, group 2 yields an FR value of 3.56. Thus, it has the highest probability of spring occurrence. Detailed results are in Tab. 15.

Paleozoic

Analysis of the FR result shows that the ratio is <1 for a slope less than <8°, indicating a low probability of spring occurrence within this slope range. The ratio is >1 for slopes more than 8°, which indicates a high probability of spring occurrence. The highest value was calculated for slope class 32.2-56.9° (2.16). Springs are most abundant in the north-west (292.5-337.5°), considering the relationship between spring occurrence and aspect. In the case of plan curvature, the results showed that the concave shape yielded the highest FR value 4.17, and convex shapes the lowest value (0.70). In the study area, where topographic elevation is between 791 m and 879 m, the FR is high (values of 1.68). Results based on distance analyses showed that FR >1 for <208 m (distance to fault), 168 – 245 m (distance to lithology borders), <237 m (distance to the river) and 221 – 268 m from distance to ridge-lines. In the case of lithology, group 1 yields an FR value of 1.73; thus, it has the highest probability of spring occurrence. Detailed results are in Table 16.

Paleogene

Analysis of the FR result shows that the ratio is <1 for a slope more than >11.9°, indicating a low probability of spring occurrence within this slope range. The ratio is >1 for slopes less than 11.8°, which indicates a high probability of spring occurrence. The highest value was calculated for slope class 4.98-8.52° (1.50). Springs are most abundant in the north-west (292.5-337.5°), considering the relationship between spring occurrence and aspect. In the case of plan curvature, the results showed that the concave shape yielded the highest FR value 4.64, and convex shapes the lowest value (0.53). In the study area, where topographic elevation is between 442 m and 551 m, the FR is high (values of 2.68). In the case of lithology, group 8 yields an FR value of 20.40; thus, it has the highest probability of spring occurrence. Detailed results are in Tab. 17.

Validation of spring potential maps

GIS tools were also used to validate potential maps. In the first step was used tools called Subset Feature (ArcGIS). The Subset Features tool splits the data into two subsets – training and test. The first subset will have L features, and the second subset will have N - L features (where N is the number of features in the original dataset). The features are split by generating random values from a uniform distribution [0,1]. 40% springs were used for the testing. To determine the accuracy of the three spring potential maps created in the current research using FR models, the relative operating characteristics (ROC) curve. A ROC curve is a graph showing the performance of a classification model at all classification thresholds. This curve plots two parameters: True Positive Rate. False Positive Rate. It is a common method to assess the accuracy of a diagnostic test (Egan 1975). The best method has a curve with the largest area under the curve (AUC); the AUC varies from 0.5 to 1.0. If the model does not predict the occurrence of the spring any better than chance, the AUC would equal 0.5. A ROC curve of 1 represents perfect prediction (Naghibi, Dashtpagerdi, 2016; Pourthagi, Pourghasemi, 2014; Nhu et al., 2020). The quantitative–qualitative relationship between AUC and prediction accuracy can be classified as follows: 0.5–0.6, poor; 0.61–0.7, average; 0.71–0.8, good; 0.81–0.9, very good; 0.91–1, excellent (Yesilnacar, 2005; Pourghasemi et al., 2012d, e; Pourthagi, Pourghasemi, 2014; Gautam, Kubota, Sapkota, et al., 2021; Pham et al., 2021). The prediction curves are shown in Fig. 11.

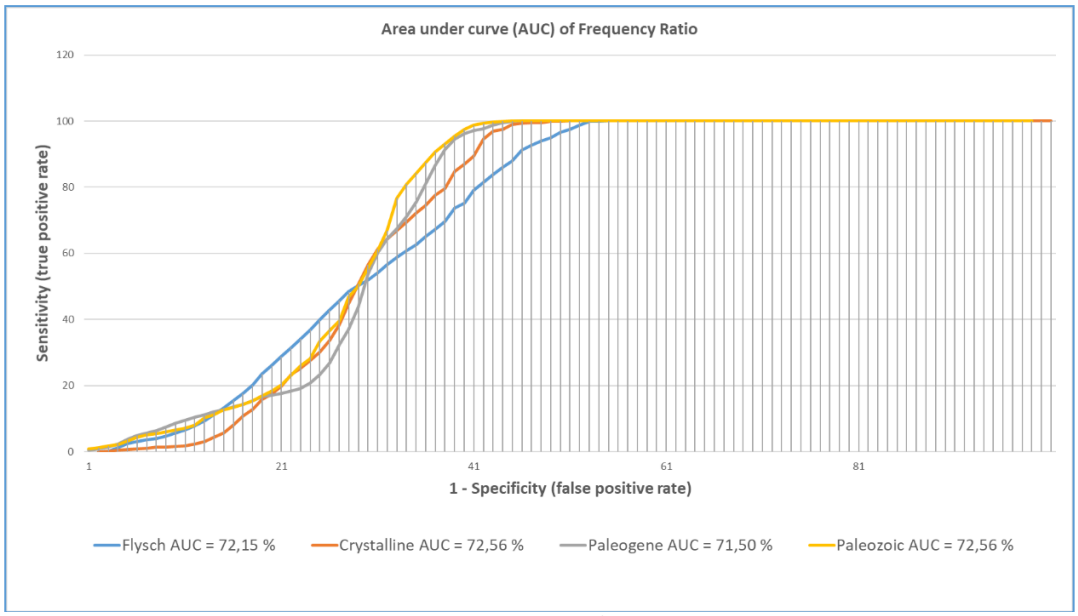

Fig. 11 AUC Excel chart between specificity and sensitivity

From Fig. 11, it is clear that in the SPM using the FR model, the AUC for the Flysch zone is 0.7215, which prepares the prediction accuracy of 72.15%; Crystalline 0.7255 (prediction accuracy = 72.55%); Paleogene 0.7151 (prediction accuracy = 71.51%) and for Paleozoic 0.7256 (prediction accuracy = 72.56%). As can be seen from the results obtained, this is a good prediction accuracy in all cases. Based on the results obtained, as well as by comparing similar works (Naghibi, Dashtpagerdi 2016; Pourthagi, Pourghasemi 2014; Nhu et al. 2020), it can be concluded that the bivariate statistical model of FR can be used as a simple tool in assessing the potential of springs if there is sufficient data. State that the bivariate statistical method provides a satisfactory combination of (subjective) professional direct mapping and (objective) analytical skills based on GIS data (Van Western et al., 1997, 2003; Pradhan et al., 2013). Bivariate statistics is a useful tool to support quantitative estimates of the importance of the relevant effectors, and a model constructed in this way allows the user to rank the importance of parameters before constructing a map of potential spring susceptibility.

Conclusion

In this study, groundwater potential zones have been identified using the FR method. In the first step, it was necessary to create a database of springs. Subsequently, fourteen data layers (slope, slope, aspect, plan curvature, elevation, topographic wetness index (TWI), stream power index (SPI), slope length (LS), lithology, distance to rivers, distance to ridge-lines, distance to faults, and distance to lithological borders were derived from a spatial database. Using the effective factors, groundwater source potential maps were created from the map index calculated using FR models, and the results were plotted in ArcGIS software. Finally, AUC curves were prepared for all areas models for testing their accuracy (Fig. 11). In all cases, the results showed that for all study areas, the values obtained were in the range of 0.71-0.8, indicating good prediction accuracy.

References

Arthur, JD., Wood, HAR., Baker, AE., Cichon, JR., Raines, GL. (2007). Development and implementation of a Bayesian-based aquifer vulnerability assessment in Florida. Nat Resour Res 16(2):93–107

Berhane, G., Kebede, M., Alfrah, N., Hagos, E., Grum, B., Giday, A., Abera, T. (2020). Landslide susceptibility zonation mapping using GIS-based frequency ratio model with multi-class spatial data-sets in the Adwa-Adigrat mountain chains, northern Ethiopia. Journal of African Earth Sciences, Volume 164, April 2020, 103795. https://doi.org/10.1016/j.jafrearsci.2020.103795

Beven K, Kirkby MJ. (1979). A physically based, variable contributing area model of basin hydrology. Hydrol Sci Bull 24:43–69

Bing, Y., Zhengxi, Y., Xiaochun, W. (2005). Applying weight of evidence to predict Pb-Zn potentia-lity in Ningnan region, Sichuan. World Geol 24(3):253–259

Blišťanová, M., Katalinic, B., Kiss, I., & Wessely, E. (2014). Data Preparation for Logistic Modeling of Flood Crisis Management. Procedia Engineering, 69, 1529-1533.

Bonham-Carter, G. F. (1994). Geographic Information Systems for Geoscientists, Modeling with GIS (398 p). Oxford: Pergamon.

Corsini, A., Cervi, F., Ronchetti, F. (2009). Weight of evidence and artificial neural networks for potential groundwater spring mapping: an application to the Mt. Modino area (Northern Apennines, Italy). Geomorphology 111:79–87

De Rosa, P., Fredduzzi, A., Cencetti, C. (2019). Stream Power Determination in GIS: An Index to Evaluate the Most 'Sensitive'Points of a River. Water 2019, 11, 1145. https://doi.org/10.3390/w11061145

Devkota, KC., Regmi, AD., Pourghasemi, HR., Yoshida, K., Pradhan, B., Ryu, IC., Dhital, MR., Althuwaynee, OF. (2013). Landslide susceptibility mapping using certainty factor, index of entropy and logistic regression models in GIS and their comparison at Mugling-Narayanghat road section in Nepal Himalaya. Nat Hazards 65(1):135–165

Egan, JP. (1975). Signal detection theory and ROC analysis. Academic, New York, pp 266–268

Ganapuram, S., Vijaya Kumar, GT., Murali Krishna, IV., Kahya, E., Demirel, MC. (2009). Mapping of groundwater potential zones in the Musi basin using remote sensing data and GIS. Adv Eng Softw 40:506–518 Geology Survey of Iran (GSI) (1997) Geology map of the Birjand Township. http://www.gsi.ir/Main/Lang_en/index.html. Accessed September 2000

Gautam, P., Kubota, T., Sapkota, L.M. et al. (2021). Landslide susceptibility mapping with GIS in high mountain area of Nepal: a comparison of four methods. Environ Earth Sci 80, 359 (2021). https://doi.org/10.1007/s12665-021-09650-2

Ghayoumian, J., MohseniSaravi, M., Feiznia, S., Nourib, B., Malekian, A. (2007). Application of GIS techniques to determine areas most suitable for artificial groundwater recharge in a coastal aquifer in southern Iran. J Asian Earth Sci 30:364–374

Ghimire, M., Chapagain, P.S. & Shrestha, S. (2019). Mapping of groundwater spring potential zone using geospatial techniques in the Central Nepal Himalayas: A case example of Melamchi–Larke area. J Earth Syst Sci 128, 26 (2019). https://doi.org/10.1007/s12040-018-1048-7

Gupta, M., Srivastava, PK. (2010). Integrating GIS and remote sensing for identification of groun-dwater potential zones in the hilly terrain of Pavagarh, Gujarat, India. Water Int 35:233–245

Haghizadeh, Ali & Davoudi Moghaddam, Davoud & Pourghasemi, Hamid. (2017). GIS-based bivariate statistical techniques for groundwater potential analysis (An example of Iran). Journal of Earth System Science. 126. 10.1007/s12040-017-0888-x.

Hickey, R. (2000). Slope Angle and Slope Length Solutions for GIS. Cartography, v. 29, no. 1, pp. 1 – 8

Hyun-Joo Oh, Yong-Sung Kim, Jong-Kuk Choi, Eungyu Park, Saro Lee (2011). GIS mapping of re-gional probabilistic groundwater potential in the area of Pohang City, Korea, Journal of Hydrology, Volume 399, Issues 3–4, 2011, Pages 158-172, ISSN 0022-1694, https://doi.org/10.1016/j.jhydrol.2010.12.027.

Hyun-Joo Oh, Biswajeet Pradhan (2011). Application of a neuro-fuzzy model to landslide-susceptibility mapping for shallow landslides in a tropical hilly area, Computers & Geosciences, Volume 37, Issue 9, 2011, Pages 1264-1276, ISSN 0098-3004, https://doi.org/10.1016/j.cageo.2010.10.012.

Chang, Y., Leng, W., He, H. (2010). Using weights of evidence to estimate the probability of forest fire occurrence: a case study in Huzhong area of the Daxingan Mountains. Sci Silvae Sinicae 46(2):103–109

Chenini, I., Ben Mammou, A. (2010). Ground water recharge study in arid region: an approach using GIS techniques and numerical modeling. Comput Geosci 36(6):801–817

Chenini, I., Ben Mammou, A., May, ME. (2010). Ground water recharge zone mapping using GIS-based multi-criteria analysis: a case study in central Tunisia (Maknassy Basin). Water Resour Mana-ge 24(5):921–939

Choi J, Oh HJ, Lee HJ, Lee C, Lee S (2012). Combining landslide susceptibility maps obtained from frequency ratio, logistic regression, and artificial neural network models using ASTER images and GIS. Eng Geol 124:12–23

Chowdhury, A., Jha, MK., Chowdary, VM., Mal, BC., 2009: Integrated remote sensing and Murthy, KSR., Mamo, AG. (2009). Multi-criteria decision evaluation in groundwater zones identifi-cation in Moyale–Teltele sub basin, South Ethiopia. Int J Remote Sens 30:2729–2740

Jaiswal, RK., Mukherjee, S., Krishnamurthy, J., Saxena, R. (2003). Role of remote sensing and GIS techniques for generation of groundwater prospect zones towards rural development: an approach. Inter J Remote Sens 24:993–1008

Jha, MK., Chowdhury, A., Chowdary, VM., Peiffer, S. (2007). Groundwater management and deve-lopment by integrated remote sensing and geographic information systems: prospects and constra-ints. Water Resour Manage 21:427–467

Káčer, Š., Antalík, M., Lexa, J., Zvara, I., Fritzman, R., Vlachovič, J., Bystrická, G., Brodnianska, M., Potfaj, M., Madarás, J., Nagy, A., Maglaj, J., Ivanička, J., Gross, P., Rakús, M., Vozárová, A., Buček, S., Boorová, D., Šimon, L., Mello, J., Polák, M., Bezák, V., Hók, J., Teťák, F., Konečný, V., Kučera, M., Žec, B., Elečko, M., Hraško, Ľ., Kováčik, M., Pristaš, J. (2005). Digitálna geologická mapa Slovenskej republiky v M 1:50 000 a 1:500 000, Bratislava:ŠGÚDŠ,Bratislava:MŽP SR, 2005. 42 s., 161 príl., 2 d., 86510

Kaliraj, S., Chandrasekar, N., Magesh, NS. (2013). Identification of potential groundwater recharge zones in Vaigai upper basin, Tamil Nadu, using GIS-based analytical hierarchical process (AHP) technique. Arab J Geosci. doi:10.1007/s12517-013-0849-x

Kayastha, P. (2015). Landslide susceptibility mapping and factor effect analysis using frequency ratio in a catchment scale: a case study from Garuwa sub-basin, East Nepal. Arabian Journal of Geosciences. 8. 10.1007/s12517-015-1831-6.

Kisss, I; Wessely, E and Blist'anova, M (2014) Contribution to Logistics of Catastrophes in Consequence of Floods. 24th DAAAM International Symposium on Intelligent Manufacturing and Automation, 2013 69 , pp.1475-1480

Lee, S., Sambath, T. (2006). Landslide susceptibility mapping in the DamreiRomel area, Cambodia using frequency ratio and logistic regression models. Environ Geol 50:847–855

Luping, P., Pengda, Z., Guangdao, H. (2008). The extended weights of evidence model using both continuous and ciscrete cata in assessment of mineral resources GIS-based. Geol Sci Technol Inform 27(6):102–106

Malík, P., Jetel, J. (1994). Metodika zostavovania hydrogeologických máp v mierke 1:50 000. Manuskript - archív Geofondu ŠGÚDŠ Bratislava, arch. č. 79616.

Malík, P., Jetel, J. (1991). Metodika zostavovania hydrogeologických máp v mierke 1:50 000. Manuskript -archív Geofondu ŠGÚDŠ Bratislava.

Minár, J., Machová, Z. (2010). Učebné texty z geomorfológie [online]. Bratislava: Univerzita Komenského v Bratislave, Prírodovedecká fakulta, 2010. [cit: 2021-05-13]. Dostupné z: http://fns.uniba.sk/Geomorfoskripta/

Mohammady, M., Pourghasemi, HR., Pradhan, B. (2012). Landslide susceptibility mapping at Go-lestan Province, Iran: a comparison between frequency ratio, Dempster–Shafer, and weights-ofevidence models. J Asian Earth Sci 61:221–236

Moore ID, Burch GJ (1986). Sediment transport capacity of sheet and rill flow: application of unit stream power theory. Water Resour Res 22(8):1350–1360

Naghbi, S. A., Dashtpagerdi, M. M. (2016). Evalution of four supervised learning methods for groundwater spring potential mapping in Khalkhal region (Iran) using GIS-based features. Hydrologeology Journal, September 2016

Nhu, V-H., Rahmati, O., Falah, F., Shojaei, S., Al-Ansari, N., Shahabi, H., Shirzadi, A., Górski, K., Nguyen, H., Ahmad, B. B. (2020). Mapping of Groundwater Spring Potential in Karst Aquifer SystemUsing Novel Ensemble Bivariate and Multivariate Models. Water 2020, 12, 985. https://doi.org/10.3390/w12040985

Nohani, E.; Moharrami, M.; Sharafi, S.; Khosravi, K.; Pradhan, B.; Pham, B.; Lee, S.; M. Melesse, A. (2019). Landslide Susceptibility Mapping Using Different GIS-Based Bivariate Models. Water 2019, 11(7), 1402; https://doi.org/10.3390/w11071402

Oh, HJ., Lee, S. (2011). Cross-application used to validate landslide susceptibility maps using a pro-babilistic model from Korea. Environ Earth Sci 64(2):395–409

Oh, HJ., Kim, YS., Choi, JK., Lee, S. (2011). GIS mapping of regional probabilistic groundwater potential in the area of Pohang City, Korea. J Hydrol 399:158–172

Ozdemir, A. (2011a) Using a binary logistic regression method and GIS for evaluating and mapping the groundwater spring potential in the Sultan Mountains (Aksehir, Turkey). J Hydrol. doi:10.1016/j.jhydrol.2011.05.015

Ozdemir, A. (2011b). GIS-based groundwater spring potential mapping in the Sultan Mountains (Konya, Turkey) using frequency ratio, weights of evidence and logistic regression methods and their comparison. J Hydrol 411:290–308

Ozdemir, A., Altural, T. (2013). A comparative study of frequency ratio, weights of evidence and logistic regression methods for landslide susceptibility mapping: Sultan Mountains, SW Turkey. J Asian Earth Sci 64:180–197

Pham, Q.B., Achour, Y., Ajim Ali, Sk., Parvin, F., Vojtek, M., Vojteková, J., Al-Ansari, N., Achu, A.L., Costache, R., Khedher, K.M., & Anh, D.T. (2021). A comparison among fuzzy multi-criteria decision making, bivariate, multivariate and machine learning models in landslide susceptibility mapping, Geomatics, Natural Hazards and Risk, 12:1, 1741-1777, DOI: 10.1080/19475705.2021.19-44330

Pengda, Z., 2007: Quantitative mineral prediction and deep mineral exploration. Earth Sci Front 14(5):1–10

Pourghasemi, HR., Pradhan, B., Gokceoglu, C., Mohammadi, M., Moradi, HR. (2012). Application of weights-of-evidence and certainty factor models and their comparison in landslide susceptibility mapping at Haraz watershed, Iran. Arab J Geosci. doi:10.1007/s12517-012-0532-7

Pourghasemi, HR., Pradhan, B., Gokceoglu, C. (2012d). Application of fuzzy logic and analytical hierarchy process (AHP) to landslide susceptibility mapping at Haraz watershed, Iran. Nat Hazards 63(2):965–996

Pourghasemi, HR., Moradi, HR., Mohammadi, M., Pradhan, B., Mostafazadeh, R., Goli Jirandeh, A., 2012e: Landslide hazard assessment using remote sensing data, GIS and weights-ofevidence model (South of

Golestan Province, Iran), Asia Pacific Conference on Environmental Science and Technology (APEST 2012), Advances in Biomedical Engineering, Volume 6, Environmental Science and Technology, 30–36

Pourghasemi, HR., Moradi, HR., Fatemi Aghda, SM. (2013c). Landslide susceptibility mapping by binary logistic regression, analytical hierarchy process, and statistical index models and assessment of their performances. Nat Hazards. doi:10.1007/s11069-013-0728-5

Pourthagi, ZS., Pourghasemi, HR. (2014). GIS-based groundwater spring potential assessment and mapping in the Bijand Township, southern Khorasan Province, Iran. Hydrogeology Journal, January 2014.

Pradhan, Biswajeet & Lee, Saro, 2010: Landslide susceptibility assessment and factor effect analysis: backpropagation artificial neural networks and their comparison with frequency ratio and bivariate logistic regression modelling. Environmental Modelling and Software. 747-759. 10.1016/j.envsoft.2009.10.016.

Pradhan, A.M.S., Dawadi, A., Kim, Y.T., 2013: Use of different bivariate statistical landslide susceptibility methods: A case study of Kulekhani watershed Nepal; J. Nepal Geol. Soc. 44 1–12.

Pradhan, B., Abokharima, M.H., Neamah Jebur, M., Shafapour Tehrany, M., 2014: Land subsidence susceptibility mapping at Kinta Valley (Malaysia) using the evidential belief function model in GIS; Nat. Hazards 73(2) 1019–1042, https://doi.org/10.1007/s11069-014-1128- 1.

Rasyid, A.R., Bhandary, N.P. & Yatabe, R., 2016: Performance of frequency ratio and logistic regression model in creating GIS based landslides susceptibility map at Lompobattang Mountain, Indonesia. Geoenviron Disasters 3, 19 (2016). https://doi.org/10.1186/s40677-016-0053-x

Regmi, AD., Yoshida, K., Pradhan, B., Pourghasemi, HR., Khumamoto, T., Akgun, A., 2013: Appli-cation of frequency ratio, statistical index and weights-of-evidence models, and their comparison in landslide susceptibility mapping in central Nepal Himalaya. Arab J Geosci. doi:10.1007/s12517-012-0807-z

Ruan S, Huang R (2001) Application of GIS-based information model on assessment of geo-logical hazards risk. J Chengdu Univ Technol 28(1):89–92

Saha, D., Dhar, YR., Vittala, SS. (2010). Delineation of groundwater development potential zones in parts of marginal Ganga Alluvial Plain in South Bihar, Eastern India. Environ Monit Assess 165:179–191

Srivastava, PK., Bhattacharya, AK. (2006). Groundwater assessment through an integrated approach using remote sensing, GIS and resistivity techniques: a case study from a hard rock terrain. Int J Remote Sens 27:4599–4620

Shahid, S., Nath, SK., Roy, J. (2000). Groundwater potential modeling in a soft rock area using a GIS. Int J Remote Sens 21(9):1919–1924

Singh, AK., Prakash, SR. (2003). An integrated approach of remote sensing, geophysics and GIS to evaluation of groundwater potentiality of Ojhala sub-watershed, Mirzapur District UP India. Remote Sensing Applications Centre, Lucknow, India

Solomon, S., Quiel, F. (2006). Groundwater study using remote sensing and geographic information systems (GIS) in the central highlands of Eritrea. Hydrol J 14:729–741

Švasta, J., Malík, P., Mižák, J. (2017). Vytváranie a odovzdávanie základných hydrogeologických máp v GIS formáte (Creation and publishing of basic hydrogeological maps in GIS format.), In: Podzemná voda v regiónoch Slovenska. Zborník príspevkov zo seminára. - Bratislava : Slovenská asociácia hydrogeológov, 2017. - ISBN 978-80-972651-0-6. - s. 18-27

Van Westen, C.J., Rengers, N., Terlien, M. T. J., Soeters, R. (1997). Prediction of the occurrence of slope instability phenomena through GIS-based hazard zonation; Geol. Rundsch. 86 404–414.

Van Westen, C.J., Rengers N., Soeters, R., 2003: Use of geomorphological information in indirect landslide susceptibility assessment. Nat Hazards 30:399–419

Vojtek, M.; Vojteková, J. (2019). Flood Susceptibility Mapping on a National Scale in Slovakia Using the Analytical Hierarchy Process. Water 2019, 11, 364. https://doi.org/10.3390/w11020364

Wu, Yanli & Li, Wenping & Wang, Qiqing & Liu, Qiangqiang & Yang, Dongdong & Xing, Maolin & Pei, Yabing & Yan, Shishun (2016). Landslide susceptibility assessment using frequency ratio, statistical index and certainty factor models for the Gangu County, China. Arabian Journal of Geosciences. 9. 10.1007/s12517-015-2112-0.

Yilmaz, I. (2009). Landslide susceptibility mapping using frequency ratio, logistic regression, artifi-cial neural networks and their comparison: a case study from Katland slides (Tokat-Turkey). Comput Geosci 35:125–1138

Yilmaz, I., (2010). Comparison of landslide susceptibility mapping methodologies for Koyulhisar, Turkey: conditional probability, logistic regression, artificial neural networks, and support vector machine. Environ Earth Sci 61(4):821–836

Yesilnacar, EK. (2005). The application of computational intelligence to landslide susceptibility mapping in Turkey, PhD Thesis, University of Melbourne, Australia, 423 pp

Yongqing, C., Jianguo, C., Xinqing, W. (2007). GIS-based integrated quantitative assessments of mineral resources. Geol Bull China 26(2):141–149

Appendix

Tab. 14 Spatial relationship between each effective factor and springs locations using FR – Flysch zone

Class Slope (Degree)	Class Pixels	% Class Pixels	Spring Pixels	% Class Pixels	FR
0-7,4	7493634	0,21	22600	0,05	0,23
7,5-15	15740142	0,44	159200	0,34	0,77
16-22	9295161	0,26	190700	0,41	*1,57*
23-29	2814276	0,08	95400	0,20	*2,59*
30-37	380649	0,01	13900	0,03	*2,79*
38-44	22213	0,00	1200	0,00	*4,12*
45-52	2432	0,00	0	0,00	0,00
53-59	363	0,00	0	0,00	0,00
60-66	32	0,00	0	0,00	0,00
Aspect					
Flat (-1)	3294793	0,09	404	0,08	0,91
North (0-22.5 and 337.5-360)	4627613	0,13	540	0,11	0,86
North-east (22.5-67.5)	4203539	0,12	498	0,10	0,88
East (67.5-112.5)	3741186	0,10	486	0,10	0,96
Southeast (112.5-157.5)	3805192	0,11	590	0,12	*1,15*
South (157.5-202.5)	4759074	0,13	689	0,14	*1,07*
South-west (202.5-247.5)	4714270	0,13	634	0,13	1,00
West (247.5-292.5)	3605893	0,10	537	0,11	*1,10*
North-west (292.5-337.5)	2997342	0,08	452	0,09	*1,12*
Plan Curvature					
Concave (<-0.05)	11453987	0,32	3055	0,63	*1,97*
Flat (-0.05 - 0.05)	9393359	0,26	731	0,15	0,58
Convex (>0.05)	14901556	0,42	1044	0,22	0,52
Elevation					
140-290	5222997	0,15	15	0,00	0,02
300-370	7419098	0,21	114	0,02	0,11
380-440	7045897	0,20	371	0,08	0,39
450-520	5554265	0,16	738	0,15	0,98
530-600	3936412	0,11	864	0,18	*1,62*
610-690	2840851	0,08	929	0,19	*2,42*
700-790	1933231	0,05	843	0,17	*3,23*
800-910	1231400	0,03	635	0,13	*3,82*
920-1200	564751	0,02	321	0,07	*4,21*
Distance to Fault					
0-640	7912812	0,22	1036	0,21	0,97
650-1300	8831864	0,25	1061	0,22	0,89
1400-200	6587344	0,18	1033	0,21	*1,16*
2100-2700	4504300	0,13	826	0,17	*1,35*
2800-3500	3068884	0,09	499	0,10	*1,20*
3600-4300	2060352	0,06	217	0,04	0,78
4400-5300	1336543	0,04	95	0,02	0,52
5400-6400	933384	0,03	47	0,01	0,37
6500-9100	448595	0,01	19	0,00	0,31
Distance to Geology					
0-140	11572545	0,32	1012	0,21	0,65
150-330	8192450	0,23	878	0,18	0,79
340-550	5700087	0,16	793	0,16	*1,03*
560-800	3970394	0,11	706	0,15	*1,32*
810-1100	2722284	0,08	606	0,13	*1,65*
1200-1400	1765467	0,05	410	0,08	*1,72*
1500-1800	974572	0,03	253	0,05	*1,92*
1900-2300	594905	0,02	137	0,03	*1,70*
2400-3700	241730	0,01	33	0,01	*1,01*
Distance to River					
1	7773936	0,22	2125	0,44	*2,02*

1,01-2	7733616	0,22	1070	0,22	*1,02*
2,01-3	6706149	0,19	652	0,14	0,72
3,01-4	5330208	0,15	460	0,10	0,64
4,01-5	3780389	0,11	291	0,06	0,57
5,01-6	2396698	0,07	166	0,03	0,51
6,01-7	1288301	0,04	57	0,01	0,33
7,01-8	574686	0,02	8	0,00	0,10
8,01-9	161419	0,00	0	0,00	0,00
Distance to Ridge					
0-28,8	11322680	0,32	43100	0,09	0,28
28,9-72,1	7662905	0,21	68600	0,14	0,66
72,2-111	5978068	0,17	96200	0,20	*1,19*
112-144	4364999	0,12	97300	0,20	*1,65*
145-178	3196547	0,09	89800	0,19	*2,08*
179-216	1971846	0,06	57200	0,12	*2,15*
217-274	1019628	0,03	27200	0,06	*1,97*
275-505	228827	0,01	3700	0,01	*1,20*
506-1230	3150	0,00	200	0,00	*4,70*
TWI					
1,65-4,75	4355457	0,12	42900	0,09	0,73
4,76-5,81	8979140	0,25	78100	0,16	0,64
5,82-6,68	10465389	0,29	153000	0,32	*1,08*
6,69-7,56	6999569	0,20	111500	0,23	*1,18*
7,57-8,72	3064064	0,09	47900	0,10	*1,16*
8,73-10,3	1124036	0,03	31400	0,07	*2,07*
10,4-12,3	436674	0,01	13000	0,03	*2,20*
12,4-14,8	230764	0,01	4400	0,01	*1,41*
14,9-26,3	93809	0,00	800	0,00	0,63
SPI					
0-4150	35545872	0,99	476200	0,99	0,99
4160-20700	168963	0,00	5900	0,01	*2,58*
20800-49800	25987	0,00	900	0,00	*2,56*
49900-91200	5409	0,00	0	0,00	0,00
91300-158000	1762	0,00	0	0,00	0,00
159000-253000	594	0,00	0	0,00	0,00
254000-382000	226	0,00	0	0,00	0,00
383000-560000	68	0,00	0	0,00	0,00
561000-1060000	21	0,00	0	0,00	0,00
LS					
0-6,92	16039194	0,45	67800	0,14	0,31
6,93-17,3	13890617	0,39	182600	0,38	0,97
17,4-31,1	4707761	0,13	157500	0,33	*2,48*
31,2-48,4	830131	0,02	46900	0,10	*4,18*
48,5-72,6	202913	0,01	16400	0,03	*5,98*
72,7-104	59489	0,00	7900	0,02	*9,83*
105-156	15651	0,00	3700	0,01	*17,50*
157-280	2786	0,00	200	0,00	*5,31*
281-882	360	0,00	0	0,00	0,00
Geology					
Group 1	10847569	0,30	137300	0,28	0,94
Group 2	5932840	0,17	19300	0,04	0,24
Group 3	2054803	0,06	5600	0,01	0,20
Group 4	4296133	0,12	2100	0,00	0,04
Group 5	6623025	0,19	99800	0,21	*1,11*
Group 6	4404435	0,12	189200	0,39	*3,18*
Group 7	979472	0,03	27500	0,06	*2,08*
Group 8	220119	0,01	2000	0,00	0,67
Group 9	366243	0,01	500	0,00	0,10

Tab. 15 Spatial relationship between each effective factor and springs locations using FR – Crystalline

Class Slope (Degree)	Class Pixels	% Class Pixels	Spring Pixels	% Class Pixels	FR
0-9,2	4035769	0,14	30600	0,16	*1,11*
9,21-14,8	6336341	0,23	58900	0,31	*1,36*
14,9-19,7	6802747	0,24	56900	0,30	*1,22*
19,8-24,3	5993456	0,22	44300	0,23	*1,08*
24,4-28,9	4691119	0,17	34000	0,18	*1,06*
29-33,8	3117535	0,11	23100	0,12	*1,08*
33,9-40,7	1599488	0,06	6500	0,03	0,59
40,8-51,9	412379	0,01	1600	0,01	0,57
52-83,7	134708	0,00	400	0,00	0,43
Aspect					
Flat (-1)	3089352	0,09	31300	0,12	*1,31*
North (0-22.5 and 337.5-360)	3707674	0,11	29100	0,11	*1,01*
North-east (22.5-67.5)	4049657	0,12	25700	0,10	0,82
East (67.5-112.5)	4071496	0,12	24300	0,09	0,77
Southeast (112.5-157.5)	4111317	0,12	27000	0,11	0,85
South (157.5-202.5)	4098277	0,12	29900	0,12	0,94
South-west (202.5-247.5)	3645904	0,11	24500	0,10	0,87
West (247.5-292.5)	3190608	0,10	31500	0,12	*1,28*
North-west (292.5-337.5)	3159257	0,10	33000	0,13	*1,35*
Plan Curvature					
Concave (<-0.05)	2903594	0,09	76700	0,30	*3,41*
Flat (-0.05 - 0.05)	26973700	0,81	167900	0,66	0,80
Convex (>0.05)	3246248	0,10	11700	0,05	0,47
Elevation					
131-458	5234007	0,16	26800	0,10	0,66
459-656	6923104	0,21	83500	0,33	*1,56*
657-844	7009854	0,21	66700	0,26	*1,23*
845-1030	5238818	0,16	41700	0,16	*1,03*
1040-1230	3313977	0,10	20200	0,08	0,79
1240-1450	2523796	0,08	13200	0,05	0,68
1460-1700	1496410	0,05	2000	0,01	0,17
1710-1990	976357	0,03	1000	0,00	0,13
2000-2660	407219	0,01	1200	0,00	0,38
Distance to Fault					
0-925	8702729	0,26	99500	0,39	*1,48*
926-1850	7548913	0,23	64000	0,25	*1,09*
1860-2770	5967478	0,18	47200	0,18	*1,02*
2780-3700	4376886	0,13	27000	0,11	0,80
3710-4620	3131409	0,09	13300	0,05	0,55
4630-5550	1974649	0,06	4200	0,02	0,27
5560-6470	1026673	0,03	1100	0,00	0,14
6480-7400	375381	0,01	200	0,00	0,07
7410-8320	4836	0,00		0,00	0,00
Distance to Geology					
0-97	11782420	0,36	82900	0,32	0,91
97,1-226	8523454	0,26	61700	0,24	0,94
227-388	5539204	0,17	38700	0,15	0,91
389-566	3448531	0,10	21800	0,09	0,82
567-776	2046170	0,06	17400	0,07	*1,10*
777-1030	1088861	0,03	14500	0,06	*1,73*
1040-1390	515245	0,02	12000	0,05	*3,02*
1400-2310	177947	0,01	6200	0,02	*4,52*
2320-4120	1059	0,00		0,00	0,00
Distance to River					
0-183	12484003	0,38	185200	0,72	*1,92*
184-504	14412965	0,44	58000	0,23	0,52
505-1010	5115715	0,15	10100	0,04	0,26

1020-2150	929095	0,03	2000	0,01	0,28
2160-4770	154548	0,00	700	0,00	0,59
4780-7060	6867	0,00		0,00	0,00
7070-8340	3548	0,00		0,00	0,00
8350-11000	3645	0,00		0,00	0,00
11100-11700	4368	0,00		0,00	0,00
Distance to Ridge					
0-24,6	8642297	0,26	14600	0,06	0,22
24,7-86-1	13033560	0,39	82200	0,32	0,81
86,2-148	7460344	0,23	103600	0,40	*1,79*
149-221	3354622	0,10	49100	0,19	*1,89*
222-381	602477	0,02	7100	0,03	*1,52*
382-762	21807	0,00	100	0,00	0,59
763-1550	5783	0,00	100	0,00	*2,23*
1560-2320	955	0,00		0,00	0,00
2330-3140	323	0,00		0,00	0,00
TWI					
0,115-4,08	3594151	0,11	18400	0,07	0,66
4,09-5,07	7324364	0,22	33600	0,13	0,59
2,08-5,87	8740710	0,26	51100	0,20	0,76
5,88-6,66	7423042	0,22	63900	0,25	*1,11*
6,67-7,55	3868651	0,12	42300	0,17	*1,41*
7,56-8,74	1372418	0,04	23800	0,09	*2,24*
8,75-10,3	481409	0,01	15000	0,06	*4,03*
10,4-12,4	218545	0,01	6800	0,03	*4,02*
12,5-25,4	100252	0,00	1400	0,01	*1,80*
SPI					
0-2330	32829749	0,99	249500	0,97	0,98
2340-9300	207441	0,01	6200	0,02	*3,86*
9310-18600	52894	0,00	500	0,00	*1,22*
18 700-31 400	20870	0,00	100	0,00	0,62
31 500-47 700	7707	0,00		0,00	0,00
47 800-68 600	3020	0,00		0,00	0,00
68 700-97 700	1294	0,00		0,00	0,00
97 800-149 000	454	0,00		0,00	0,00
150 000-297 000	113	0,00		0,00	0,00
LS					
0 - 7,18	9078832	0,27	52600	0,21	0,75
7,19 - 21,5	13719762	0,41	102700	0,40	0,97
21,6 - 39,5	7687713	0,23	63900	0,25	*1,07*
39,6 - 61	1953824	0,06	23900	0,09	*1,58*
61,1 - 93,3	445058	0,01	8900	0,03	*2,58*
93,4 - 133	151362	0,00	3000	0,01	*2,56*
134 - 183	61075	0,00	900	0,00	*1,90*
184 - 266	22070	0,00	400	0,00	*2,34*
267 - 915	3846	0,00		0,00	0,00
Geology					
Group 1	5861669	0,18	10500	0,04	0,23
Group 2	3534935	0,11	97400	0,38	*3,56*
Group 3	3980393	0,12	67500	0,26	*2,19*
Group 4	2523180	0,08	32900	0,13	*1,69*
Group 5	4694025	0,14	11900	0,05	0,33
Group 6	3493374	0,11	1700	0,01	0,06
Group 7	4271714	0,13	6600	0,03	0,20
Group 8	2462252	0,07	1900	0,01	0,10
Group 9	2252720	0,07	25300	0,10	*1,45*

Tab. 16 Spatial relationship between each effective factor and springs locations using FR – Paleozoic

Class Slope (Degree)	Class Pixels	% Class Pixels	Spring Pixels	% Class Pixels	FR
0 - 8,03	724103	0,10	5900	0,06	0,60
8,04 - 12,5	1437996	0,19	20000	0,20	*1,03*
12,6 - 16,1	1817424	0,25	32300	0,32	*1,32*
16,2 - 19,2	1828806	0,25	41200	0,41	*1,67*
19,3 - 22,1	1569840	0,21	36800	0,37	*1,74*
22,2 - 25	1216002	0,16	29700	0,30	*1,81*
25,1 - 28,1	867409	0,12	18700	0,19	*1,60*
28,2 - 32,1	462005	0,06	8700	0,09	*1,40*
32,2 - 56,9	123570	0,02	3600	0,04	*2,16*
Aspect					
Flat (-1)	879610	0,09	26600	0,14	*1,54*
North (0-22.5 and 337.5-360)	1063929	0,11	20500	0,10	0,98
North-east (22.5-67.5)	1280174	0,13	26000	0,13	*1,04*
East (67.5-112.5)	1241416	0,12	24200	0,12	0,99
Southeast (112.5-157.5)	1230804	0,12	16900	0,09	0,70
South (157.5-202.5)	1227110	0,12	14000	0,07	0,58
South-west (202.5-247.5)	1096570	0,11	13100	0,07	0,61
West (247.5-292.5)	1038915	0,10	23100	0,12	*1,13*
North-west (292.5-337.5)	988627	0,10	32500	0,17	*1,68*
Plan Curvature					
Concave (<-0.05)	453236	0,05	37000	0,19	*4,17*
Flat (-0.05 - 0.05)	9063567	0,90	152600	0,78	0,86
Convex (>0.05)	530352	0,05	7300	0,04	0,70
Elevation					
233 - 437	761215	0,08	4600	0,02	0,31
438 - 535	1407742	0,14	14100	0,07	0,51
536 - 620	1620766	0,16	24800	0,13	0,78
621 - 705	1650315	0,16	29200	0,15	0,90
706 - 790	1469558	0,15	39400	0,20	*1,37*
791 - 879	1225986	0,12	40400	0,21	*1,68*
880 - 977	934133	0,09	23900	0,12	*1,31*
978 - 1 100	645485	0,06	15900	0,08	*1,26*
1 110 - 1 320	331955	0,03	4600	0,02	0,71
Distance to Fault					
0 - 208	3101767	0,31	107400	0,54	*1,76*
209 - 451	2541467	0,25	39900	0,20	0,80
452 - 746	1787890	0,18	26500	0,13	0,75
747 - 1 080	1085263	0,11	13600	0,07	0,64
1 090 - 1 440	674703	0,07	6900	0,03	0,52
1 450 - 1 860	406463	0,04	2300	0,01	0,29
1 870 - 2 360	273852	0,03	700	0,00	0,13
2 370 - 3 140	151078	0,02		0,00	0,00
3 150 - 4 430	14699	0,00		0,00	0,00
Distance to Geology					
0 - 41,7	3282247	0,33	67100	0,34	*1,04*
41,8 - 99	2654913	0,26	55800	0,28	*1,07*
99,1 - 167	1864033	0,19	33800	0,17	0,93
168 - 245	1119113	0,11	24400	0,12	*1,11*
246 - 339	629343	0,06	10100	0,05	0,82
340 - 453	304681	0,03	4200	0,02	0,70
454 - 609	130801	0,01	1000	0,01	0,39
610 - 870	45195	0,00	300	0,00	0,34
871 - 1 330	16737	0,00		0,00	0,00
Distance to River					
0 - 237	4155841	0,41	144300	0,73	*1,77*
238 - 474	3426845	0,34	35800	0,18	0,53
475 - 771	1840105	0,18	13100	0,07	0,36

772 - 1 360	540932	0,05	3500	0,02	0,33
1 370 - 2 730	63492	0,01		0,00	0,00
2 740 - 4 240	4734	0,00		0,00	0,00
4 250 - 5 010	7134	0,00		0,00	0,00
5 020 - 6 110	1834	0,00		0,00	0,00
6 120 - 7 560	2744	0,00		0,00	0,00
Distance to Ridge					
0 - 28,1	2538878	0,25	8200	0,04	0,16
28,2 - 63,8	2404961	0,24	17000	0,09	0,36
63,9 - 102	1903425	0,19	31800	0,16	0,85
103 - 140	1364716	0,14	46900	0,24	*1,76*
141 - 179	902264	0,09	43500	0,22	*2,46*
180 - 220	552325	0,05	29300	0,15	*2,71*
221 - 268	261077	0,03	14800	0,08	*2,90*
269 - 342	101445	0,01	4600	0,02	*2,32*
343 - 651	17294	0,00	600	0,00	*1,77*
TWI					
-10,7 - 0,156	10034120	1,00	196900	1,00	*1,00*
0,157 - 1,96	10834	0,00		0,00	0,00
1,97 - 3,24	1112	0,00		0,00	0,00
3,25 - 4,4	567	0,00		0,00	0,00
4,41 - 5,43	371	0,00		0,00	0,00
5,44 - 6,59	95	0,00		0,00	0,00
6,6 - 8	46	0,00		0,00	0,00
8,01 - 10,2	10	0,00		0,00	0,00
SPI					
0 - 2 350	9955209	0,99	187500	0,95	0,96
2 360 - 9 380	62933	0,01	7800	0,04	*6,32*
9 390 - 18 800	19203	0,00	1600	0,01	*4,25*
18 900 - 30 500	6242	0,00		0,00	0,00
30 600 - 46 900	2307	0,00		0,00	0,00
47 000 - 70 400	815	0,00		0,00	0,00
70 500 - 104 000	285	0,00		0,00	0,00
105 000 - 155 000	124	0,00		0,00	0,00
156 000 - 299 000	37	0,00		0,00	0,00
LS					
0 - 7,06	2289432	0,23	19200	0,10	0,43
7,07 - 18,8	4133835	0,41	59800	0,30	0,74
18,9 - 30,6	2416447	0,24	59200	0,30	*1,25*
30,7 - 44,7	868850	0,09	34600	0,18	*2,03*
44,8 - 65,9	220923	0,02	12400	0,06	*2,86*
66 - 94,2	70718	0,01	6600	0,03	*4,76*
94,3 - 129	32239	0,00	3400	0,02	*5,38*
130 - 186	12775	0,00	1500	0,01	*5,99*
187 - 600	1936	0,00	200	0,00	*5,27*
Geology					
Group 1	1296471	0,13	44100	0,22	*1,73*
Group 2	1252495	0,12	31100	0,16	*1,27*
Group 3	1787679	0,18	26600	0,14	0,76
Group 4	1272544	0,13	40100	0,20	*1,61*
Group 5	662376	0,07	10700	0,05	0,82
Group 6	548255	0,05	4800	0,02	0,45
Group 7	1622080	0,16	17400	0,09	0,55
Group 8	1234168	0,12	16500	0,08	0,68
Group 9	360627	0,04	5600	0,03	0,79

Tab. 17 Spatial relationship between each effective factor and springs locations using FR – Paleogene

Class Slope (Degree)	Class Pixels	% Class Pixels	Spring Pixels	% Class Pixels	FR
0 - 4,97	3877031	0,16	5000	0,19	*1,18*
4,98 - 8,52	5962735	0,25	9800	0,37	*1,50*
8,53 - 11,8	5857743	0,24	7000	0,27	*1,09*
11,9 - 14,9	4572115	0,19	4400	0,17	0,88
15 - 18,2	3675244	0,15	2300	0,09	0,57
18,3 - 21,5	2446672	0,10	2200	0,08	0,82
21,6 - 25,1	1527641	0,06	1600	0,06	0,96
25,2 - 29,8	838430	0,04	100	0,00	0,11
29,9 - 60,3	238104	0,01		0,00	0,00
Aspect					
Flat (-1)	3153271	0,11	4200	0,13	*1,19*
North (0-22.5 and 337.5-360)	3544710	0,12	2900	0,09	0,73
North-east (22.5-67.5)	3446153	0,12	3300	0,10	0,86
East (67.5-112.5)	3046494	0,11	2700	0,08	0,79
Southeast (112.5-157.5)	3053636	0,11	3400	0,10	1,00
South (157.5-202.5)	3412274	0,12	4200	0,13	*1,10*
South-west (202.5-247.5)	3248353	0,11	3200	0,10	0,88
West (247.5-292.5)	3051740	0,11	3800	0,12	*1,11*
North-west (292.5-337.5)	3039084	0,10	4700	0,15	*1,38*
Plan Curvature					
Concave (<-0.05)	1099905	0,04	5700	0,18	*4,64*
Flat (-0.05 - 0.05)	26708958	0,92	26000	0,80	0,87
Convex (>0.05)	1186852	0,04	700	0,02	0,53
Elevation					
108 - 309	2532952	0,09	5300	0,16	*1,87*
310 - 441	2788897	0,10	4500	0,14	*1,44*
442 - 551	4278497	0,15	12800	0,40	*2,68*
552 - 652	4412768	0,15	4700	0,15	0,95
653 - 747	4964319	0,17	2600	0,08	0,47
748 - 836	3688713	0,13	1000	0,03	0,24
837 - 937	3362581	0,12	1100	0,03	0,29
938 - 1 050	1965990	0,07	400	0,01	0,18
1 060 - 1 450	1000998	0,03		0,00	0,00
Distance to Fault					
0 - 536	9896085	0,34	13200	0,41	*1,20*
537 - 1 270	8743831	0,30	7900	0,25	0,81
1 280 - 2 080	4793708	0,17	4600	0,14	0,86
2 090 - 3 010	2741925	0,09	1200	0,04	0,39
3 020 - 4 150	1470991	0,05	2600	0,08	*1,59*
4 160 - 5 630	768966	0,03	700	0,02	0,82
5 640 - 7 900	357488	0,01	1400	0,04	*3,53*
7 910 - 10 600	111933	0,00	500	0,02	*4,02*
10 700 - 17 100	35956	0,00		0,00	0,00
Distance to Geology					
0 - 81,5	10968884	0,38	21100	0,68	*1,79*
81,6 - 199	8043699	0,28	6000	0,19	0,70
200 - 335	4453722	0,15	2700	0,09	0,57
336 - 489	2440991	0,08	500	0,02	0,19
490 - 670	1446162	0,05	800	0,03	0,52
671 - 897	855015	0,03		0,00	0,00
898 - 1 180	444753	0,02		0,00	0,00
1 190 - 1 550	239994	0,01		0,00	0,00
1 560 - 2 310	100597	0,00		0,00	0,00
Distance to River					
0 - 253	11244063	0,39	16300	0,51	*1,31*
254 - 695	12108175	0,42	9900	0,31	0,74
696 - 1 330	3758895	0,13	3800	0,12	0,91

1 340 - 2 150	1214046	0,04	1600	0,05	*1,19*
2 160 - 3 160	393879	0,01	500	0,02	*1,14*
3 170 - 4 610	176251	0,01	100	0,00	0,51
4 620 - 6 820	61451	0,00		0,00	0,00
6 830 - 10 000	27713	0,00		0,00	0,00
10 100 - 16 100	6385	0,00		0,00	0,00
Distance to Ridge					
0	2224573	0,08	400	0,01	0,16
0,001 - 96,5	18251585	0,63	11000	0,34	0,54
96,6 - 386	8444043	0,29	20000	0,62	*2,13*
387 - 772	60944	0,00	500	0,02	*7,39*
773 - 1 250	9587	0,00	300	0,01	*28,18*
1 260 - 2 220	2585	0,00		0,00	0,00
2 230 - 3 570	171	0,00		0,00	0,00
3 580 - 6 180	150	0,00		0,00	0,00
6 190 - 24 600	196	0,00		0,00	0,00
TWI					
-12,4 - -0,0541	28487133	0,98	31500	0,97	0,99
-0,054 - 1,63	464600	0,02	800	0,02	*1,54*
1,64 - 2,89	39395	0,00	100	0,00	*2,27*
2,9 - 4,01	2981	0,00		0,00	0,00
4,02 - 4,99	1166	0,00		0,00	0,00
5 - 6,11	249	0,00		0,00	0,00
6,12 - 7,51	142	0,00		0,00	0,00
7,52 - 9,62	49	0,00		0,00	0,00
SPI					
0 - 1 110	28806354	0,99	31600	0,98	0,98
1 120 - 5 570	146835	0,01	800	0,02	*4,88*
5 580 - 13 400	30511	0,00		0,00	0,00
13 500 - 24 500	7884	0,00		0,00	0,00
24 600 - 41 200	2939	0,00		0,00	0,00
41 300 - 67 900	918	0,00		0,00	0,00
68 000 - 116 000	221	0,00		0,00	0,00
117 000 - 198 000	46	0,00		0,00	0,00
199 000 - 284 000	7	0,00		0,00	0,00
LS					
0 - 4,46	11221970	0,39	13100	0,40	*1,04*
4,47 - 11,2	9360249	0,32	10000	0,31	0,96
11,3 - 20,1	5520414	0,19	5800	0,18	0,94
20,2 - 31,2	2124903	0,07	2800	0,09	*1,18*
31,3 - 44,6	547295	0,02	500	0,02	0,82
44,7 - 64,7	155654	0,01	100	0,00	0,57
64,8 - 93,7	49468	0,00	100	0,00	*1,81*
93,8 - 147	14392	0,00		0,00	0,00
148 - 569	1370	0,00		0,00	0,00
Geology					
Group 1	21450249	0,74	15400	0,49	0,66
Group 2	1925449	0,07	2800	0,09	*1,33*
Group 3	1364171	0,05	5300	0,17	*3,55*
Group 4	824906	0,03	500	0,02	0,55
Group 5	448875	0,02	400	0,01	0,81
Group 6	748426	0,03	1200	0,04	*1,46*
Group 7	538176	0,02	2800	0,09	*4,75*
Group 8	147641	0,01	3300	0,10	*20,40*
Group 9	1480822	0,05		0,00	0,00